T.C.

ALTINBAS UNIVERSITY

Institute of Graduate Studies

Mechanical Engineering

NUMERICAL INVESTIGATION OF HEAT TRANSFER, PRESSURE DROP, AND EXERGY FOR PHE USING NANOFLUIDS

Hatem Shaban Mesbah SHINKADA

Master of Science

Supervisor

Asst. Prof. Dr. Ibrahim KOÇ

Istanbul, 2021

NUMERICAL INVESTIGATION OF HEAT TRANSFER, PRESSURE DROP, AND EXERGY FOR PLATE HEAT EXCHANGER USING NANOFLUIDS

by

Hatem Shaban Mesbah SHINKADA

Mechanical Engineering

Submitted to the Graduate School of Science and Engineering

in partial fulfillment of the requirements for the degree of

Master of Science

ALTINBAŞ UNIVERSITY

2021

The thesis titled "NUMERICAL INVESTIGATION OF HEAT TRANSFER, PRESSURE DROP, AND EXERGY FOR Plate Heat Exchanger USING NANOFLUIDS" prepared and presented by Hatem Shaban Mesbah SHINKADA was accepted as a Master of Science Thesis in Mechanical Engineering.

____

Asst. Prof. Dr. Ibrahim KOÇ

Supervisor

Thesis Defense Jury Members:

Asst. Prof. Dr. Ibrahim KOÇ	School of Engineering and Architecture, Altinbas University	_________________
Asst. Prof. Dr.Süleyman BAŞTÜRK	School of Engineering and Architecture, Altinbas University	_________________
Prof. Dr. Haydar UYANIK	School of Applied Sciences, KTO Karatay University	_________________

I certify that this thesis satisfies all the requirements as a thesis for the degree of Master of Science.

Approval Date of Institute of Graduate Studies: ____/____/____

I hereby declare that all information in this document has been obtained and presented in accordance with academic rules and ethical conduct. I also declare that, as required by these rules and conduct, I have fully cited and referenced all material and results that are not original to this work.

Hatem Shaban Mesbah SHINKADA

DEDICATION

Great thanks to Allah. I really want to give special thanks to my first instructors, my parents, who were also my first role models and supporters along the trip, as well as my brothers. This dream would never come true if it weren't for you.

ACKNOWLEDGEMENTS

I'd want to definite my thankfulness to everyone who has sustained me during this journey, which has lasted for a long time. I'd need to thank my adviser, Asst. Prof. Dr. Ibrahim KOÇ, for his compass even when I thought I was misplaced and for being an outstanding portion of the effort's pinnacle. I'd also like to express my gratitude to my boss for his encouraging words, which significantly improved the quality of this project. Finally, I want to definite my gratefulness to this institution for greeting me throughout the years and firmly establishing itself such as my family. I am grateful to my parents, whose beliefs and education inspire me to ask questions for relatives and family for their unconditional love; and to my nation, that, while being inanimate, keeps me grounded and serves as a case of resiliency.

ABSTRACT

NUMERICAL INVESTIGATION OF HEAT TRANSFER, PRESSURE DROP, AND EXERGY FOR PLATE HEAT EXCHANGER USING NANOFLUIDS

SHINKADA, Hatem Shaban Mesbah

M.Sc., Mechanical Engineering, Altınbaş University,

Supervisor: Asst. Prof. Dr. Ibrahim KOÇ

Date: October/2021

Pages: 58

In this thesis, a numerical investigation has been presented on the Plate Heat Exchanger (PHE) using Tin nanofluid with water. Reynolds numbers have been changed to study *Nu*, *f*, and exergy loss. Finite volume method has been utilized for the numerical investigation and the simulation results have been confirmed with the previous experimental result. Influences of dissimilar operating factors for example weight concentration of nanofluid in the hot side and *Re* from 2540 to 12700 have been studied on *U*, *Nu*, and *f*, and temperature, velocity, and pressure distribution. The results showed that the *U* increased with the rise of *Re*s and weight fraction of nanoparticles where the nanofluids with 0.5% concentration achieved the highest values and the enhancement ratio %age start from 123.5%-133.5%. *Nu* enhance with the increase of the Reynold number and volume concentration of nanofluids where the 0.5 weight concentration (wt. %) Tin-water nanofluid scores the highest values of *Nu* from 43 to 68. The *f* decreases with the increase of *Re* where the case of 0.6% concentration Tin to water recorded the extreme *f* with values from 0.18 to 0.35. The exergy loss of nanofluid with different concentrations increases with the growth of *Re* and the concentration of 0.5 wt. % Tin –water achieved the highest exergy loss following the numbers from 50 to 66. Streamlines and contours of temperature, velocity, and pressure distribution inside the PHE give reliable explanations for the motion of cold and hot water and heat transfer enhancement.

Keywords: Plate Heat Exchanger, Heat transfer, Pressure drop, Nanofluids, Numerical study

TABLE OF CONTENTS

Pages

LIST OF TABLES

Pages

LIST OF FIGURES

Pages

LIST OF ABBREVIATIONS

FPHE	:	Flat PHE
CFD	:	Computational Fluid Dynamics
PHE	:	Plate heat exchanger
LMTD	:	Logarithmic mean temperature

LIST OF SYMBOLS

A	:	Surface area, m^2
$\dot{m}$	:	Mass flow rate, kg/s
D_h	:	Hydraulic diameter, m
T	:	Temperature, ◦C
C_p	:	Specific heat, J/kg.K
Q	:	Heat transfer rate, W
g	:	Gravity acceleration, m/s^2
p	:	Pressure, Pa
U	:	Overall heat transfer coefficient, W/m^2K
u	:	Velocity, m/s
h	:	Heat transfer coefficient, J/kgK
T_o	:	Ambient temperature, °C
S	:	Entropy, J/kgK
f	:	Friction factor
k	:	Thermal conductivity, W/mK
Re	:	Reynolds number
ΔP	:	Pressure drop, Pa
μ	:	Viscosity , Ns/m^2
ρ	:	Density of water , kg/m^3

SUBSCRIPTS

E	:	Exergy loss
out	:	Out
in	:	In
ave	:	Average
c	:	Cold water
h	:	Hot water
surr	:	Surrounding
β	:	Corrugation angle

1. INTRODUCTION

One of the most basic consequences on industrial applications and human lives is the problem of thermal energy storage. As a result, a great deal of attention must be paid to improving energy efficiency and performance. The most well-known utilizing of energy transfer for cooling and heating, as well as other chemical processes, is the heat exchanger. In thermal systems, energy savings can be attained by adjusting the thermophysical parameters of the working fluid or modifying the design of heat exchangers.

1.1 HEAT EXCHANGER

This is a device that transmits thermal power between two or more liquids, gases, a solid faces and fluids, or between fluid and solid particles, at varied temperatures and in thermos interaction, while no external heat or work interactions are present.

1.2 CLASSIFICATION OF HEAT EXCHANGER

As presented in Figure 1.1, heat exchangers are classified based on a variety of factors including the transfer method, liquid phase, flow arrangement, location, and shape. There are two styles of heat transfer processes (direct and indirect). In direct contact, the cold and hot liquids mix more tightly, allowing heat to flow from an upper temperature to a lesser temperature. The fluid streams stay distinct in indirect contact, and heat is transmitted constantly through an impermeable splitting wall or rapidly into and out of a wall. As a result, in an ideal environment, thermally reacting fluids should not come into direct touch with one another. A surface heat exchanger is another name for that sort of heat exchanger. Conferring to the flow direction (counter fluid flow, parallel flow, and cross flow), there are three types of heat exchangers as seen in Figure 1.1[1]. In the parallel fluid flow, both fluid flows in the similar path. Both fluids, on the other hand, flow in opposing paths. Some tapes are denoted as horizontal heat exchangers, while others are referred to as vertical heat exchangers.

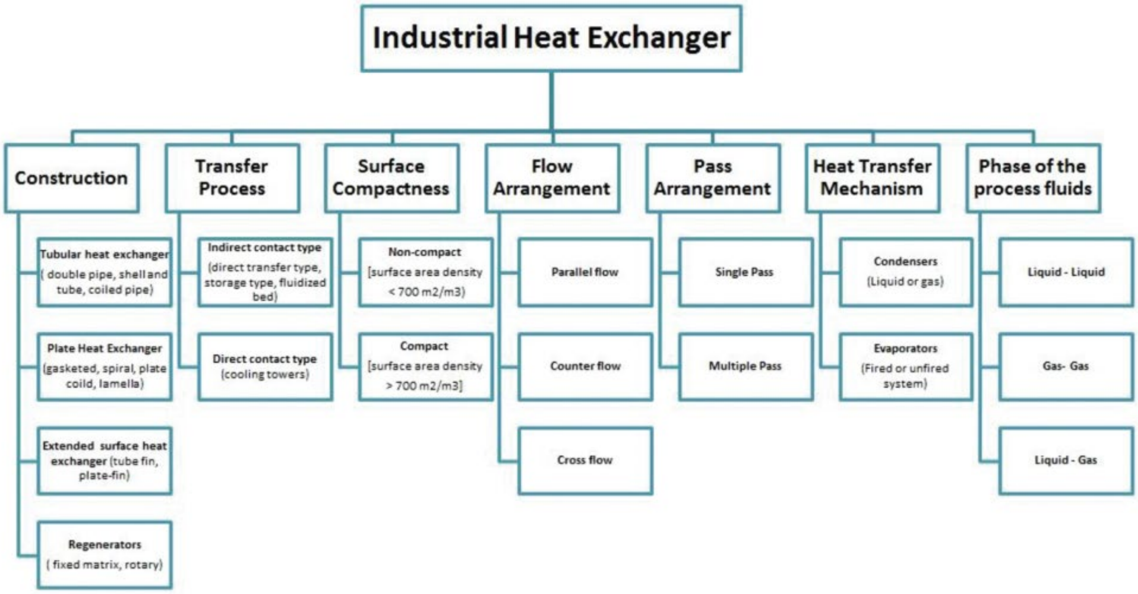

Figure 1.1: Classification of industrial heat exchanger [1]

1.3 PLATE HEAT EXCHANGER

PHEs were originally manufactured in the 1920s and are now widely employed in a variety of industries. As shown in Figure 1.2, a PHE is a form of heat exchanger that procedures metallic plates to transmit the heat from fluid to other. The fluids are subjected to a much larger surface area than in a traditional heat exchanger becautilizing they extend out over the plates. This enhances the rate of temperature change by speeding up the heat transfer mechanism.

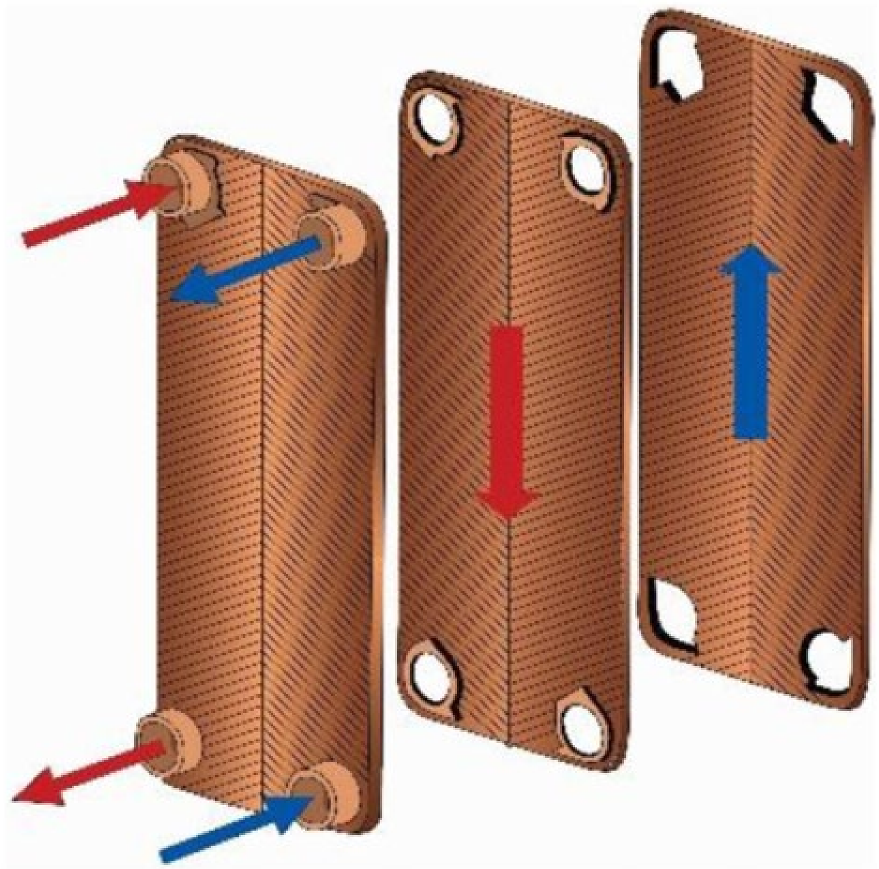

Figure 1.2: Flow directions in the PHE[2]

Millions of combination boilers utilizing extremely small brazed PHEs in the hot-water sections. Due to their high heat transfer efficiency for such a small physical size, the domestic hot water flowrate of combination boilers has increased. The tiny PHE has had a considerable impact on domestic heating and hot water. Gaskets are utilized between the plates in larger commercial models, whereas brazing is utilized in smaller versions. A heat exchanger works by transferring heat between one fluid and another using pipes or other containment devices. In most cases, the exchanger is made up of a coiled pipe that transports one fluid through a chamber that transports another fluid. To assist the exchange, the pipe walls are normally composed of metal or a different material that have higher thermal conductivity, whilst the outside large chamber covering is usually finished from plastic or thermal protection coating to avoid heat escaping from the heat exchanger.

1.3.1 Plate heat exchanger classification

There are many types of PHE such as brazed PHE, gasketed PHE, and PHE spare parts. The brazed can be classified into fusion -bonded brazed PHE, and nickel brazed PHE.

1.3.2 Advantages of Plate heat exchanger

There are many advantages of PHE like flexibility, good temperature control, efficient heat transfer and low manufacturing cost that can be illustrated in this section.

1.3.2.1 Flexibility

PHEs can be easily adapted to changing procedure necessities by basically addition or deleting plates, or altering the figure of passes, thanks to simple disassembly. Furthermore, the range of plate corrugation patterns available, as well as the ability to combine them in the same PHE, allows for the testing of multiple unit conformations during optimization methods [2].

1.3.2.2 Good temperature control

Becautilizing of the thin passages created among consecutive plates, single a minor amount of liquid is trapped in a PHE. As a result, the tool reacts fast to procedure situations changes and has small gap times, making temperature management simple. Avoiding high temperatures is crucial. Besides, channel shapes decreases the probability of dead regions forming [2].

1.3.2.3 Low manufacturing cost

Because the plates are forced together relatively than welding, PHE manufacturing can be comparatively cheap. During the production process, specific materials may be utilized to make the plates further resilient to erosion and chemical reaction[5].

1.3.2.4 Efficient heat transfer

The plates' corrugations and the tiny hydraulic radius aid in the creation of turbulence flow, allowing for significant heat transfer rates for the fluids. As a result, up to 90% of the heat can be recovered, whereas shell-and-tube heat exchangers can only recover 50% of the heat.

1.3.2.5 Compactness

PHEs have a very tiny footprint due to their excellent thermal efficacy. When comparing to shell and tube heat exchangers, PHEs can take up to 80% less floor space for the similar heat transfer zone.

1.3.2.6 Reduced fouling

Fouling is reduced due to the mixture of a little fluid residence period and great turbulence. PHEs can have 10 times lower scale factors than shell and tube heat exchangers. It's easy to inspect and clean: All portions exposed to fluids can be cleaned and inspected becautilizing the PHE parts may be disconnected. This quality is crucial in food activities. De leakage is simple.

1.3.3 Disadvantages of PHE

1.3.3.1 Temperature and pressure limitations

The plate seals remain a substantial constraint for PHEs. Where temperatures and pressures more than 160 °C and 25 atm, respectively, are not accepted later the typical gaskets leaks. Gaskets constructed of specific materials, on the other hand, can endure temperatures of up to 400°C, and the plates can be welded or brazed together to work in even harsher conditions. Becautilizing gaskets are no longer required, this would have the added benefit of expanding operational limits and allowing for the utilizing of corrosive fluids [3].

1.3.3.2 High pressure drop

Since the crenelated plates and the tiny flows area among them, there is a significant pressure loss owing to friction, that growths pump prices. It can be explained that the pressure loss may be decreased by growing the figure of passes to each passes and excruciating the stream obsessed by multiple channels. By lowering the velocity inside the passage, the f is reduced. The U, on the other hand, is reduced, lowering the heat exchanger's effectiveness.

1.3.3.3 Phase change

PHEs may be utilized in condensing or evaporating processes in some conditions, however becautilizing of the partial area inside the passages and pressure limits, they are not advised for gases and vapors.

1.3.3.4 Types of fluids

Becautilizing of the significant related ΔP and flow delivery subjects within the PHE, processing fluids which have excessively viscous or contain fibrous material is not suggested. The fluid's compatibility with the gasket material should also be addressed. Becautilizing of the risk of leaking, extremely combustible or hazardous fluids need be escaped.

1.3.3.5 Leakage

Resistance among the metallic plates might result in garb and the creation of minor, difficult-to-find holes. It's a good idea to pressurize the process fluid as a precaution to reduce the possibility of contamination in the case of a plate leak.

1.3.4 PHE arrangement

The simple PHE systems are in that together liquids create single pass and the flows do not change direction. Single-pass configurations are divided into two categories: countercurrent and concurrent. The fluid entrances and outputs may be fitted in the permanent plate of the single-pass configuration, making opening the tools for repairs and washing easier without disrupting the piping work. The U arrangement, which is the widely utilized only passage design, is the most widely utilized single pass design. As shown in Figure 1.3, a lone pass Z-configuration with fluid input and output over end plates is found.

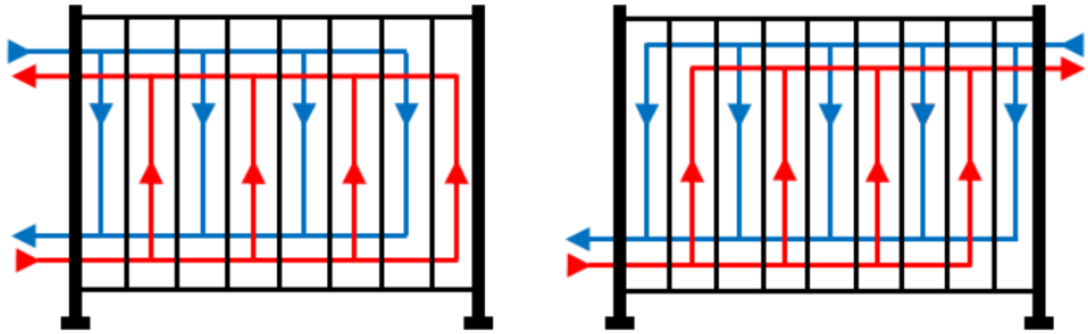

Figure 1.3 Configurations of a simple-pass PHE. (a) U-configuration and (b) Z-configuration[3]

Counter current flow, in which the streams movement in reverse directions, is favored over concurrent flow, in which the streams go in the similar direction, since it achieves superior thermal efficiency. Multi-pass systems is utilized to increase flow velocity and heat transmission of the streams, and are typically necessary when the stream rates of the flows differ significantly, as shown in Figure 1.4.

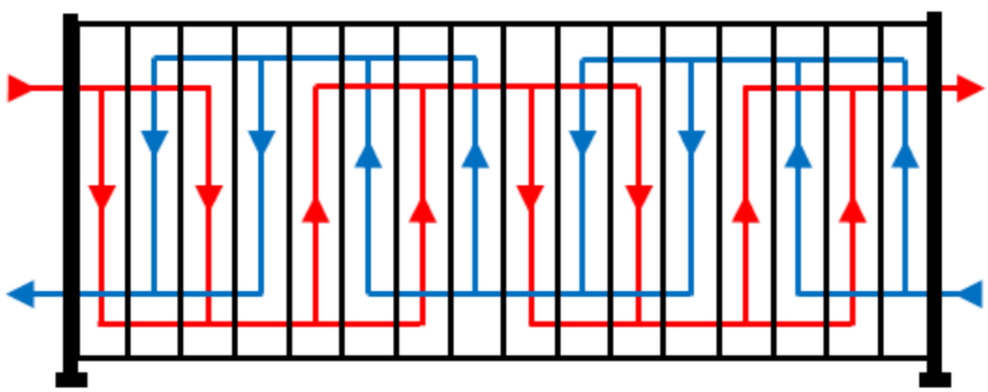

Figure 1.4: Multi-pass PHE [3]

1.3.5 PHE structure

A PHE features a frame with a heavy moving component that slips beside a carrying or controlling bar and one fixed heavy front piece with four openings. A number of fastening bolts path down the side of each weighty plates, where a different number of plates are put and secured together. Each plate is fitted with a gasket, forming a locked scheme of flow networks that permits the main and minor fluids to pass through every other plate. As shown in Figure 1.5, the gaskets are clipped or attached onto the plates separating distinct Medias on the primary and secondary circuits.

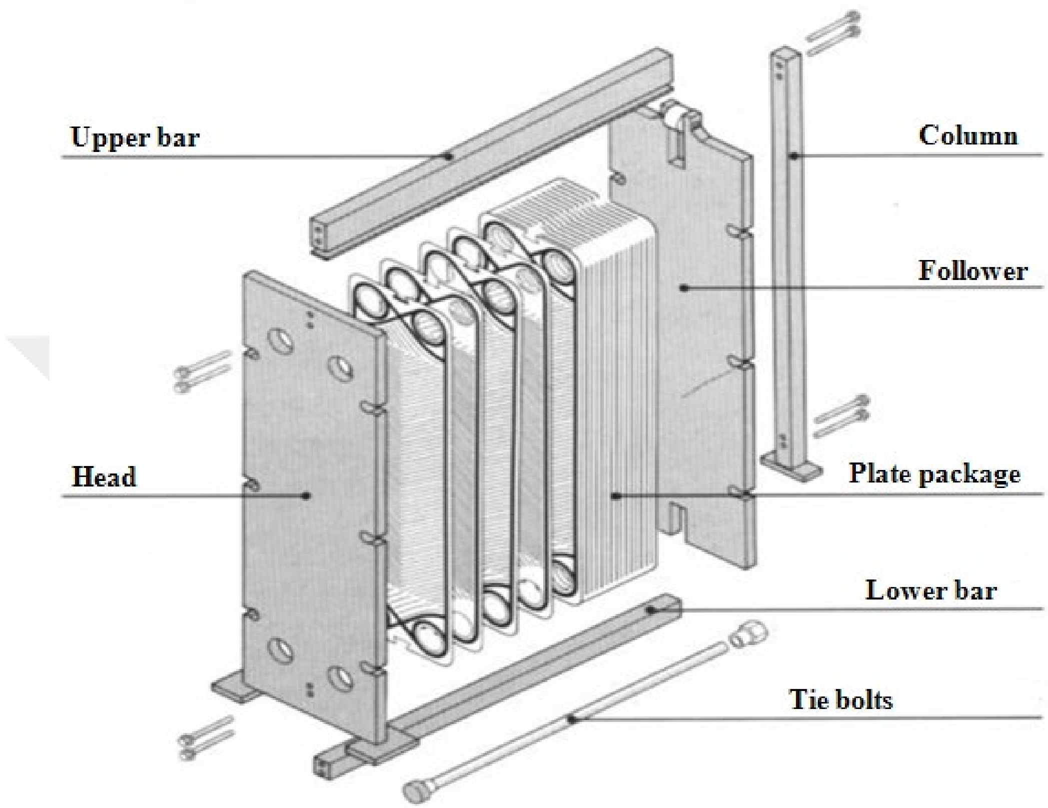

Figure 1.5: The structure of PHE [4]

2. LITERATURE REVIEW

2.1 INTRODUCTION

Plate heat exchangers were developed through the 1930s to encounter the dairy industry's hygienic requirements and are now the most common heat transfer machines. Since of their many benefits, for example compact size and weightiness, great thermal effectiveness, hygienic fittingness, flexibility, and easiness of hygiene, in addition to higher thermal performance, PHEs are extensively utilized in numerous industrial applications.

Stoitchkov and Dimitrov [5] produced a small cut technique for the measurement of heat exchangers for wet surface crossflow plate quality. This involves a correction to the effectiveness determined in compliance with the Maclaine cross and Banks procedure. For this reason, a new model has been developed with a moving water film, referring to the actual situations in the heat exchangers. The approach to the measurement of the mean temperature of the surface of the water and the equation derivation to calculate the fraction of gross to rational heat, in view of the atmospheric pressure, improves the Maclaine-cross and Banks process.

Das and Roetzel [6] completed a second law study via a PHE for thermally dispersive flow. Back mixing and other differences in plug flow are well known to substantially contribute to the heat exchanger incompetence in the plate fin or PHEs, which is of concern for heat exchangers employed in the cryogenic management. It is observed that the conventional axial heat spreading scheme is superior to the plug flow scheme, however still inacceptable wherever the time scale associated with heat transfer is similar to the time of thermal reduction for the transmission of dispersion.

In a individual passage U-type counter-flow PHE, Muley and Manglik [7] examined three distinct chevron plate configurations. Water was utilized for testing runs with a scale from 2 to 6 for the Prandtl number (Pr) and 600 to 10^4 for the *Re* important effects of the chevron angle and surface area enlargement component were seen in the results. The heat transference was observed to be enhanced by up to 2, 8 times that of an analogous flat-plate channel at constant pumping capacity.

Saman and Alizadeh [8] looked at how efficient a cross flow PHE is such as a dehumidification and unintended evaporation cooler. One stream of air is covered with a fluid desiccant mixture, though evaporation is utilizingd to cool the other stream. The outcomes specified a significant association between the field of heat and mass transfer, the concentration of the solution, and the secondary to primary relation of mass flow rate of air. The output of a counterflow and a parallel flow configuration did, however, show minor variations. The suggested absorber does not adjust for either the latent or allowable main air load.

Krishna Kumar et al. [9] did a thorough investigation of the effects of stream misdistribution from passage to passage. This raises main concerns regarding the standard approach of analyzing PHE experimental heat transfer data. It was determined how important it is to consider the U in the passages as a function of mass stream rate. This solves the inconsistency of different stream rates however the same heat transfer coefficients. As shown in Figure 2.1, a broad range of parametric studies have been provided, highlighting impacts such as the heat capability rate percentage, flow design, channels figure, and number of transfer unit NTU. The effectiveness variation versus the number of transfer units can be explained in this figure where the effectiveness enhanced with the rise of the NTU and flow-distribution parameter played vital role on effectiveness. The results of this study point to a more accurate technique of analyzing heat transfer statistics for PHEs.

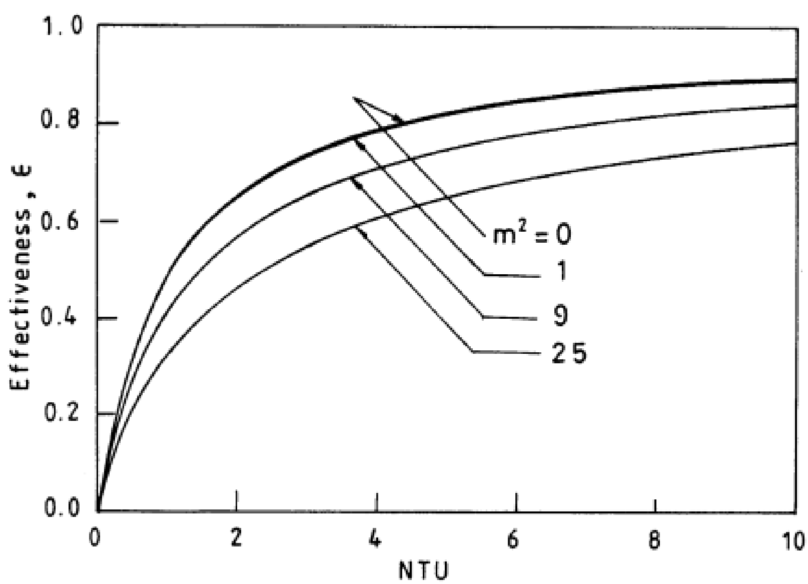

Figure 2.1: The effects of number of transfer units on the effectiveness [9]

Ayub [10] proposed an exploration on PHEs and introduced novel correlations for the coefficient of f and evaporative heat transfer applicable to different conditions of device pressure and plate chevron angles. The similarities are established on real field data gathered through the construction and operation of chillers for many years.

Ding et al. [11] examined the effect of temperature on the effective thermal conductivity of CNT nanofluids and studied the mechanisms for thermal-conduction enhancement in CNT nanofluids. The operational thermal conductivity rises as the temperature rises, with a nonlinear relationship between the two. The thermal-conductivity enhancement has an essentially linear relationship with temperature for temperatures below 30 ºC, while the relationship tends to level off above around 30 ºC. The macroscopic models were unable to anticipate the increase in heat conductivity accurately.

High temperatures, it was concluded, could cautilizing dispersant failure and, as a result, nanofluid destabilization. Temperature should not exceed 60 ºC –70 °C for nanofluids prepared with SDBS. Koo and Kleinstreue [12] utilized numerical methods to investigate the effects of copper oxide nanospheres in water and ethylene glycol at low volume concentrations on the heat transfer problem for microheat sinks. New designs are utilizingd to estimate nanofluids' improved thermal conductance and kinematic viscosity. To reduce nanoparticle deposition, large Prandtl number carrier fluids were utilizingd, and also nanoparticles at large volume densities of about 4%, higher thermal high conductivity and dielectric constants adjacent the liquid medium, microchannels with high surface areas, and regarded path surface.

Using computational fluid dynamics, Miura et al. [13] created an effective sample of a four channel PHE with smooth plates. It was verified in parallel and series stream configurations, and the outcome was associated with statistical heat loads projections from a three dimensional CFD prototype and a single dimensional plug stream prototype. The model incorporates the exchanger's channels, plates, and conduits, as well as the differential stream distributions across passages and stream maldistribution in the tube. The CFD outcomes, especially for series arrangements, are in respectable accord with investigational outcomes.

Longo and Gasparella [14] discussed the experimental heat transfer figures and ΔP evaluated as through evaporation of HFC refrigerants 410A, 134a, and 236fa in a narrow brazed PHE, including the result of heat and refrigerant fluid mass fluxes, temperature gradient, exhaust situations, and flow situations. The coefficients of heat transfer also on refrigeration sides and the frictional *ΔP* are provided in the experimental findings. The frictional pressure decrease is proportional to the refrigeration flow's kinetic energy of the system. Heat transfer factors are 40% to 50% greater in HFC-410A than in HFC-134a and 50% to 60% upper in HFC-236fa, and resistance pressure decreases are 40% to 50% lower in HFC-410A than in HFC-134a and 50% to 60% lower in HFC-236fa. The heat transfer factors are highly sensitive to heat flow and external situations, but only somewhat sensitive to saturation temperature.

Warnakula and Worek [15] looked at the *ΔP* and the heat transfer factor. The shift to turbulent movement happens at *Re*s is lower at 10 to 400, according to the findings. As a result, PHEs attain excellent overall heat transfer factors, lower fouling rates, and overall size reduction even at modest velocities. Extraordinary heat transfer rates are obtained in reasonably narrower flow pathways with high heat transfer coefficients, resulting in a smaller overall dimension and *ΔP*. The *Re* was altered from 250 to 1100 in the hot salt solution side, resulting in a *Nu* ranging from 7.4 to 15.8 as seen in Figure 2.2.

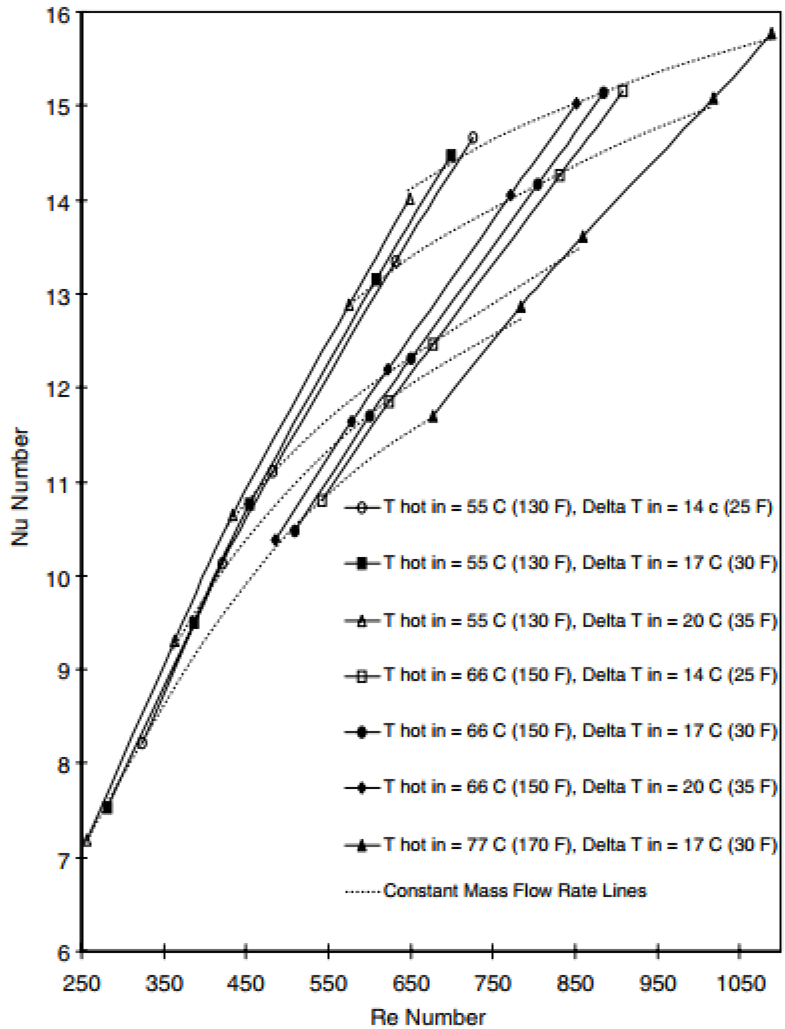

Figure 2.2: *Nu* variation with *Re* of solution at various intake temperatures and inlet temperature discrepancies [15]

Mouza et al. [16] proposed a way for design and optimization of a PHE with chest heaved surfaces while adhering to quality requirements. The conceptual prototype is a 3D thin passage with angle like triangular waves in a herringbone shape, with geometric variables such as blockage percentage, passage and corrugation aspect percentage, attack angle, and *Re*. To keep the simulations number to a minimum, the Box Behnken method is utilized. An impartial purpose that blends heat transfer increase with friction losses linearly, by means of an allowance feature that accounts for energy costs, is utilized using reaction surface technique for the optimization process.

Jeng et al. [17] utilized a straight combination approach to make alumina/water nanofluid occupied fluid in the multi-passages heat exchanger. Nanofluids of various mass densities (0, 0.5, and 1.0 wt. %) as well as the inter temperature at various flow rates were utilized as experimental variables. Greater nanoparticle concentrations resulted in a higher heat transfer factor. Once the likelihood of nanoparticles colliding with the heat exchanger wall was increased under larger concentrations, the heat transfer coefficient ratio was upper, indicating that nanofluids have a lot of promise for usage in electronic chips as shown in Figure 2.3.

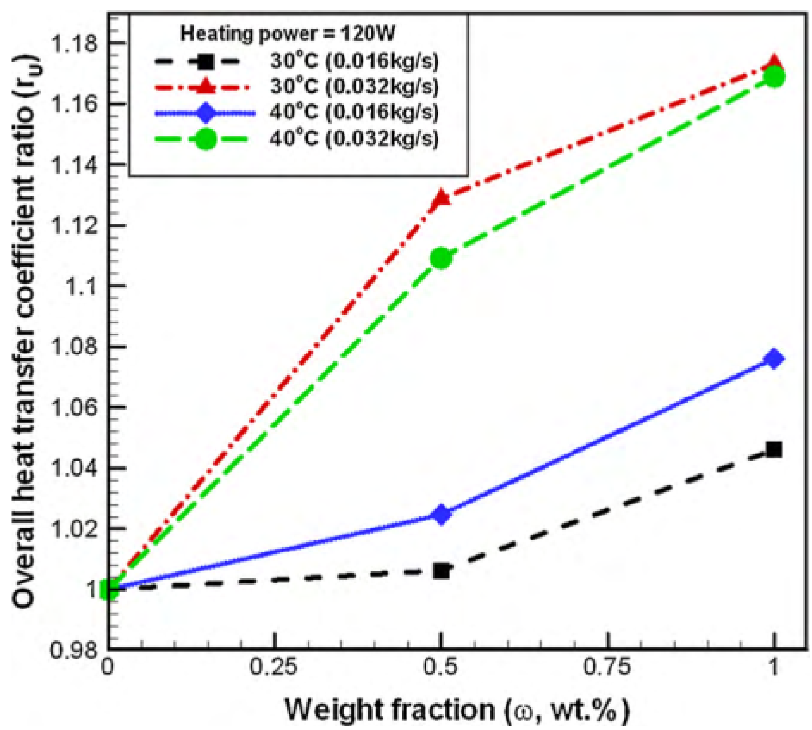

Figure 2.3: Various weight %ages of Al_2O_3/water nanofluid and different flow rates cautilizing variations in total heat transfer ratios. [17]

Shuaib et al. [18] studied the special influences of nanofluid stream on *ΔP* and heat transmission in a corrugated station statistically. The research includes the number of Reynolds and the fraction of nanoparticle volume in the 100-1000 and 0-0.05 scales, respectively. There is a small improvement in the enhancement for Re more than 200 with the increase in the number of Reynolds although a slim drop in heat transfer improvement for Re more than 200 as the number of Reynolds increases is found. The largest increase in heat transmissions were observed at *Re* of 200 and 5 % nanoparticle size fraction, through an increase of about 43.9 % above the basic fluid, for the cases studied. The study indicated that it is possible to suggest the utilizing nanofluid inside corrugated passages as an effective approach to achieving better efficiency in heat transfer that leads to the construction of extra compacted heat exchangers.

Nguyen et al. [19] determined the compulsory heat transmission and hydraulic features of a chevron style double passage manufacturing PHE while utilized through a nanofluid. He for the nanofluid side, data was collected for two size fractions of 2% and 4.65%, as well as a *Re* range of up to 1000. CuO and water nanofluid obviously demonstrates a larger *f* than water for a given *Re*, according to the findings. When employing the 2% nanofluid, *Nu*s calculated showed no substantial heat transfer increase. In spite of 4.65% nanofluid concentration, there is a decrease in transferred heat. For the nanofluids examined, the laminar-turbulent transition was also found.

Ghosh et al. [20] examined the heat transfer rate of the PHE by means of a variety of nanofluids (CeO_2, TiO_2, Al_2O_3, and SiO_2) at varying size stream rates and densities. The optimal densities for various nanofluids were also identified, resulting in the greatest heat transfer improvement. The required thermos-physical characteristics of the nanofluids were defined previous the experiments. The heat transfer coefficient, ΔP fraction, effectiveness fraction, pumping power fraction, and performance index precentage have all been discussed. Figure 2.4 shows the variability in the U of Al_2O_3 and water mixture at varied cold stream rates and size concentrations. The work presented that CeO_2 and water produces finest enhancement where the supreme performance index improvement was 16% with moderately lesser optimal density was 0.75 vol.% within studied nanofluids.

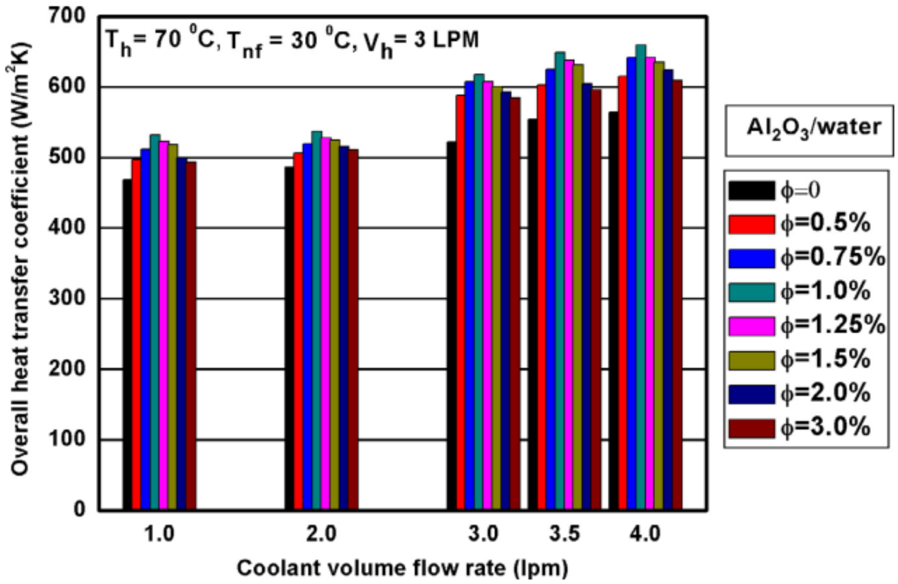

Figure 2.4: Variability in the total heat transfer coefficient of Al_2O_3/water nanofluid at varied cold flow rates and volume concentrations [20]

Ghosh et al. [21] predicted the augmentation of heat transfer for PHEs using nanofluid as a 3D CFD model coolant that reflects additional composite and functional geometries of the regions of fluid circulation. The findings revealed that the plate's corrugation pattern cautilizings fluid instability that results in high rates of heat transfer. Inside the inner cold liquid about the minor intake, the extreme temperature occurs everywhere the higher port while the lowermost temperature seems, the temperature variation is higher, and the heat transfer effect is additional acceptable. As a coolant, CeO_2 and water recorded the finest results.

Tiwari et al. [22] attempted to provide a review of numerous experimental and analytical studies carried out over the years in this area, which non-single installed a novel period of study however too established the basis for evaluating the efficiency and non-efficiencies of PHEs in different differential settings and parameters, with or without operating on and with nanofluids. The emphasis of our study is those studies that have an effect and effects on the development of a new dimension of operating on the PHE model.

In a chevron corrugated PHE, Wu et al. [23] looked into the heat transport and *ΔP* properties of a hybrid nanofluids made up of nanoparticles of alumina and multi walled carbon nanotubes (MWCNTs). A modest quantities of MWCNTs were inserted to rise the thermal conductivity of the mixture. The findings of the nanofluid combination were compared to the Al_2O_3 and water nanofluid. The *U* of hybrid nanofluid combination is somewhat greater than with the Al_2O_3 with water nanofluid and fresh water once compared heat transfer coefficients basing with similar stream speed. The combination of the hybrid nanofluid still has the maximum *U* for a specific pumping power. The *ΔP* of the hybrid nanofluid combination is lesser than the Al_2O_3 with water nanofluid and only marginally higher than that of water, as illustrated in Figure 2.5. As a result, hybrid nanofluid mixtures can be beneficial in an extensive range of heat transfer applications.

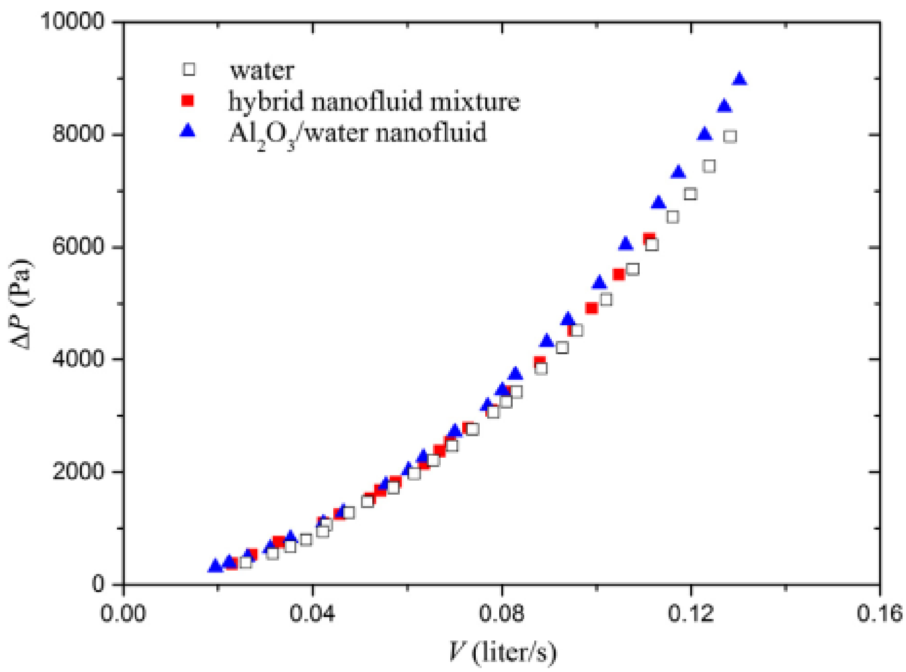

Figure 2.5: Predicted *ΔP* versus the volume flow rates **[23]**

In an experimental PHE , Tiwari et al. [24] examined the heat transferred and exergetic nanofluid performance. CeO_2/water and ZnO/water are the two types of nanofluids utilized. The outcomes of the experiments are matched to those of water and nanofluids. The ZnO/water nanofluid demonstrated the finest heat transfer show in the experiments. The nanofluids' volume concentration ranged from 0.5 to 2.0 %. At 2 LPM of warm fluid, the coolant flow rates of mixed starting 0.5.0 to 2.0 LPM. Cold and hot fluids have intake temperatures of 25° C and 50° C, correspondingly. Figure 2.6 shows the exergy losses versus water volume flow rates and various nanofluids.

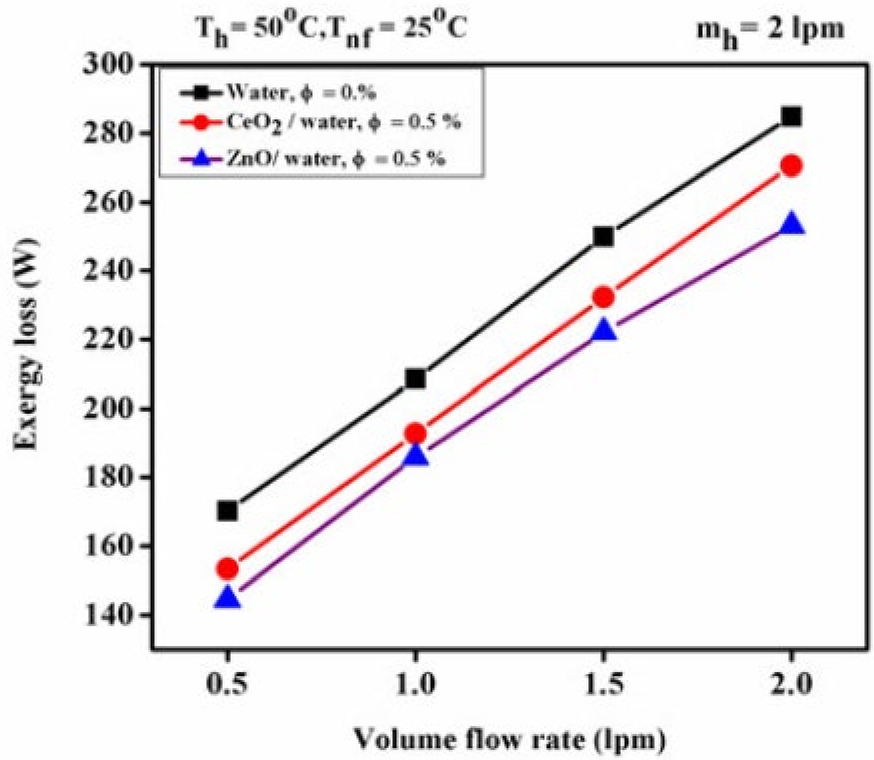

Figure 2.6: Exergy loss varies with water volume flow rates and various nanofluids. [24]

Naghizadeh et al. [25] inspected the influence of silver-water nanofluid nanofluid on PHEs with different volume flow rates and concentrations ranging from 0 to 10 mg/L. The findings show that increasing the concentration of nanofluid and volume stream ratio improves PHE's heat transfer rate. Volume flow rate, in contrast, has a higher influence on improving the total heat transfer rate than the concentration of the nanofluid. Furthermore, the ratio of heat transfer extended its extreme at a serious nanofluid concentration (2.5 mg/L). Thermal conductivity first rose as the quantity of silver nanoparticles inside the water increased, peaking at around 2.5 mg/L. In this condition, the thermal conductivity of silver water nanofluid is 36.6 % higher than that of clean water. Though, at large concentrations, the effective thermal conductivity falls owing to aggregation and a reduced area-to-volume proportion (A/V). In addition, when concentration increased, the rate of temperature increase and Brownian motion increased. The findings of conductivity and temperature rise are superimposed to prove the presence of a critical concentration for silver-water nanofluid.

Ajarostaghi et al. [26] looked at how utilizing different nanofluids as a cooling fluid affected the thermal efficiency of the Pillow PHE quantitatively. The heat transmission and *ΔP* of three water based nanofluids, involving Al_2O_3, CuO, and TiO_2, are thus investigated. Turbulence is the fluid flow, and measurements are taken at various *Re*s ranging from 1000 to 8000. The outcomes reveal that growing the concentration of nanoparticle volume in the range of 2-5 % increases the heat transfer factor significantly at a low *Re*. The outputs ratio factor is utilized to evaluate the structural device's heat transfer and *ΔP* at the same time.

Lee et al. [27] analyzed single-phase shell and PHE output with acceptable chevron angles (β) of 45º and 75º, respectively. In the shell channel, the flow pattern and the distribution of temperature are usually additional identical than those in the internal channel. Once the Re is weak, the shell channel with *f*=45º produces the best overall output because of its much lower. Once the chevron angle is sufficient, the heat transmission effectiveness of the shell pipeline far outweighs that of the inner channel (75º). The ratio of the corrugation determines the efficiency of heat transmission, and an ideal ratio is determined.

Shah et al. [28] explored the utilizing of various geometries of PHE nanofluids. In each segment, a detailed table provides essential details about nanoparticle scale, base fluids, systematic techniques, heat transfer augmentation, flow scheme, and *ΔP*. Besides, all the experiments, theoretic, investigational, and mathematical, were eventually established to offer wanted and considerable thermal efficiency comparative to traditional fluids. The statistical study for the previous published papers was also stated by the scientist, and the findings indicate the increasing significance of the presentation of nanofluids in PHEs. When compared to base fluids, most studies found that preferred thermal activity, improved heat transport, reduced entropy formation, and reduced exergy destruction. A rise in the *Re* might result in improved heat transfer ratio. The effective nanofluids temperature shows a critical part in the performance of heat exchangers and heat transfer improvement. Virtually completely experiments have shown that nanofluids have a higher thermal activity in the PHE than the base fluid, but the Chevron and Corrugated form geometry of the PHE offers a significant increase in Nusselt numbers.

Islam et al. [29] suggested a novel flow technique to improve the flat PHE's thermal efficiency (FPHE). The fundamental and modified FPHEs were utilized to run the total simulations. Physical testing are conducted in both HEs under comparable geometrical circumstances. Nu, Stanton number (St), Colburn factor j, f, and overall thermal and hydraulic performance (JF) factor are all utilized to assess and analyze the thermal efficiency of the HEs given. For spans ranging from 250 to 2000, data on heat transfer for a single process and *Re* are acquired. The numerical conclusions were validated by using benchmark experimental evidence from the literature. The upgraded FPHE's Nu and *f* values are up to 70% and 4.4 periods those of the plain FPHE, according to the findings. It specifies the revised FPHE's essential *Re*s. In compared to the basic FPHE, the revised FPHE JF data shows a 0.7 % -9 % increase in thermal efficiency, suggesting that it might protect material and power for the similar heat cability. In the current investigation, the relevant correlations for Nu and *f* for both situations have also been found.

Verma et al.[30] studied the influences of several concentrations of nanofluids of graphene oxide experimentally and computationally in compact PHE. He introduced an experimental and numerical efficiency analysis by means of graphene oxide nanofluids at varying concentrations and flow speeds. The numerical and experimental outcomes were related and found to be in good contract with both outcomes. The findings showed a 13% increase in thermal conductivity, a 14% heat transfer rate (HTR), an efficiency rate of 9% and an regular heat transfer factor of 10 % at the expense of ΔPs and nanofluid pumping capacity. Exergy loss besides declined at the maximum concentration of 1 volume fraction % using nanofluid.

2.2 THE NOVELTY OF THE STUDY

In the previous literature review, many experimental studies investigated the performance of PHE but less numerical researches studied the PHE performance. Nanofluids have a great effect on performance so that researchers did many works on this enhancement experimentally. Many materials were utilized as nanofluids to increase heat transfer but titanium nitride (Tin) was not utilized. The heat transfer and ΔP were investigated in limited *Re* ranges. No study investigated the second law of exergy for the PHE. Few studies investigated the performance of PHEs in the turbulent region. Study the effects of nanofluids as titanium nitride on the heat transfer and ΔP performance for the PHE have been studied numerically with exergy investigation with a range of *Re* from 2540 to 12700.

3. NUMERICAL STUDY

3.1 PHE MODELING

PHE consists of front and rare covers with plates and gaskets distributed uniformly in the distance between the covers as seen in Figure 3.1. The flows of the hot and cold fluids are counter flow and the inlets and outlets of waters are illustrated in the same figure.

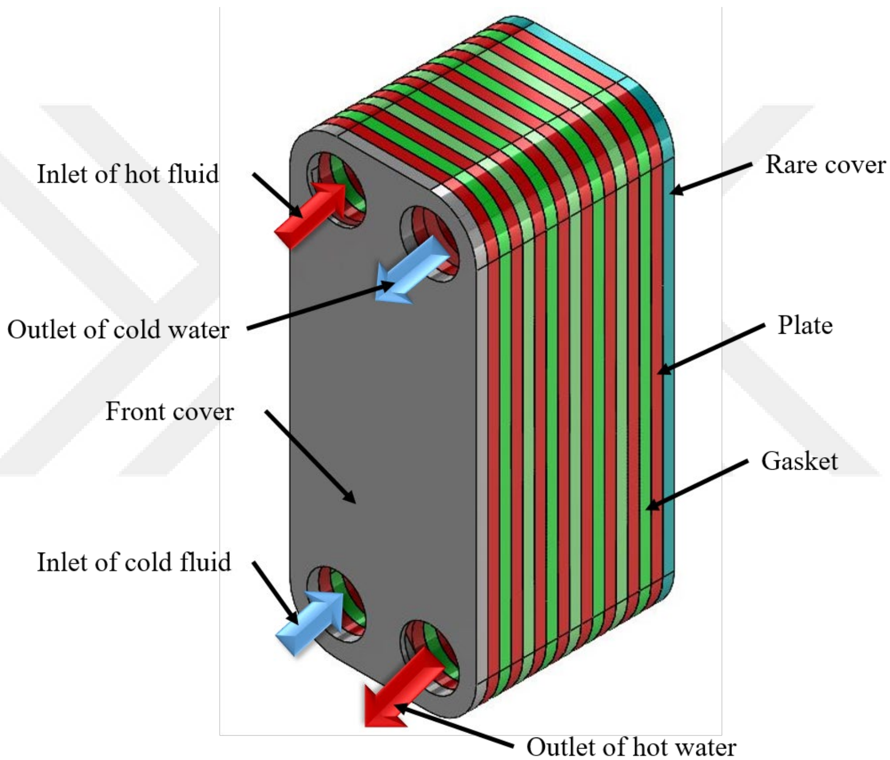

Figure 3.1: Schematic view of components of PHE

Figure 3.2 shows domains of hot and cold water as well as copper plates and gaskets. Computer Aided Design (CAD) software is utilized to complete the modeling of the PHE and internal domains.

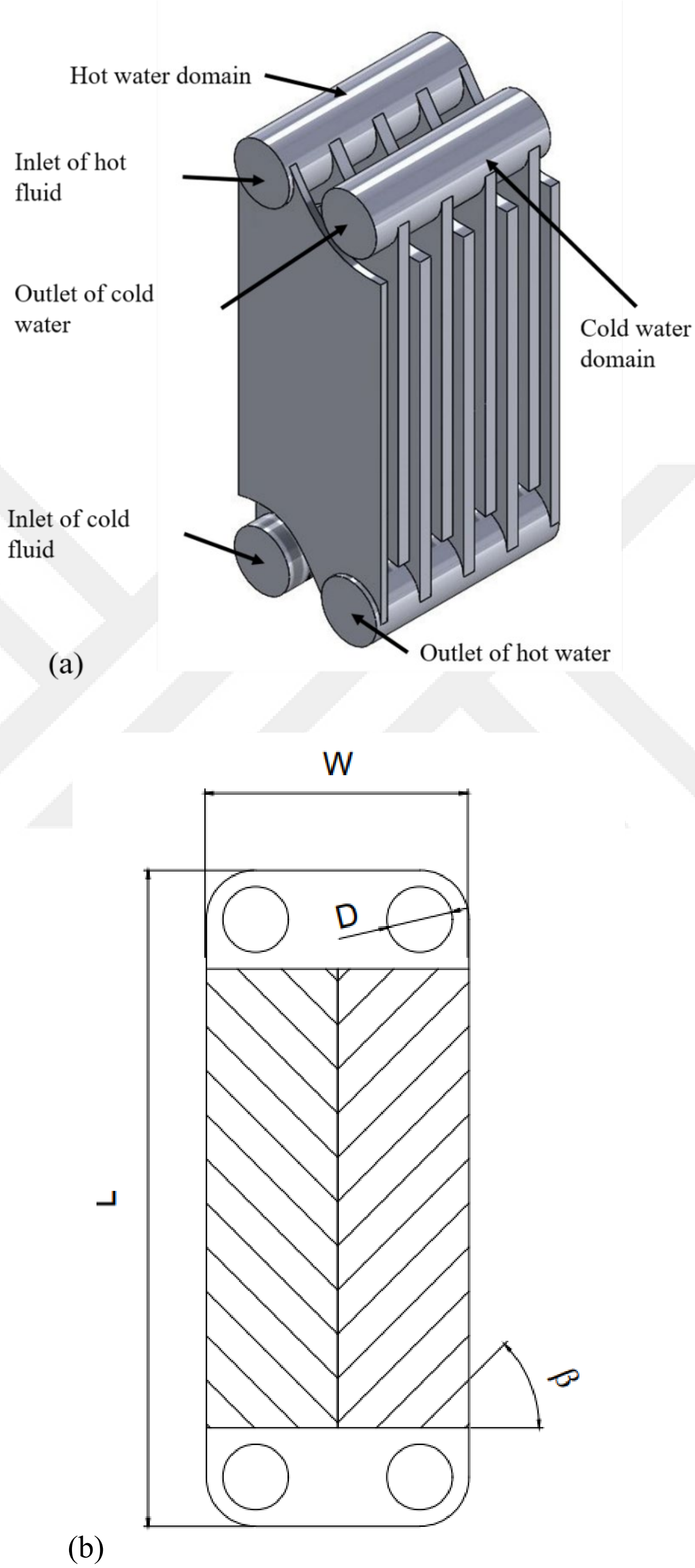

Figure 3.2: PHE (a) three dimensions domains of cold and hot water domains (b) dimensions of the plate

Table 1 illustrates the conditions and dimensions of the PHE are similar to the model utilized in [31].

Table 1: Specifications of the PHE

Parameters	Dimensions
Angle of corrugation, **β**	45°
Pitch of corrugation, **t**	8 mm
Number of the corrugated plate, **N**	8
Plate length, **L**	194 mm
Plant width, **W**	80 mm

3.2 NANO-FLUID PROPERTIES

The properties of materials that are utilized as nanoparticles in the hot side to enhance the heat transfer during the cooling or heating process are illustrated in Table 2.

Table 2: Properties of titanium nitride nanoparticles [32]

Material	Values
Chemical form	Tin
Size of the particle (nm)	30
Density (kg/m^3)	5400
Specific heat (J/kgK)	217
Thermal conductivity (W/mK)	62

3.3 MESH GENERATION

A computer software program [33] is utilized to generate an unstructured mesh of the cold and hot water domains with plates and gaskets. Figure 3.3 shows the mesh generation of the model where there is a refinement in regions besides the wall of plates and gaskets to rise the grids quality generation and simulation results.

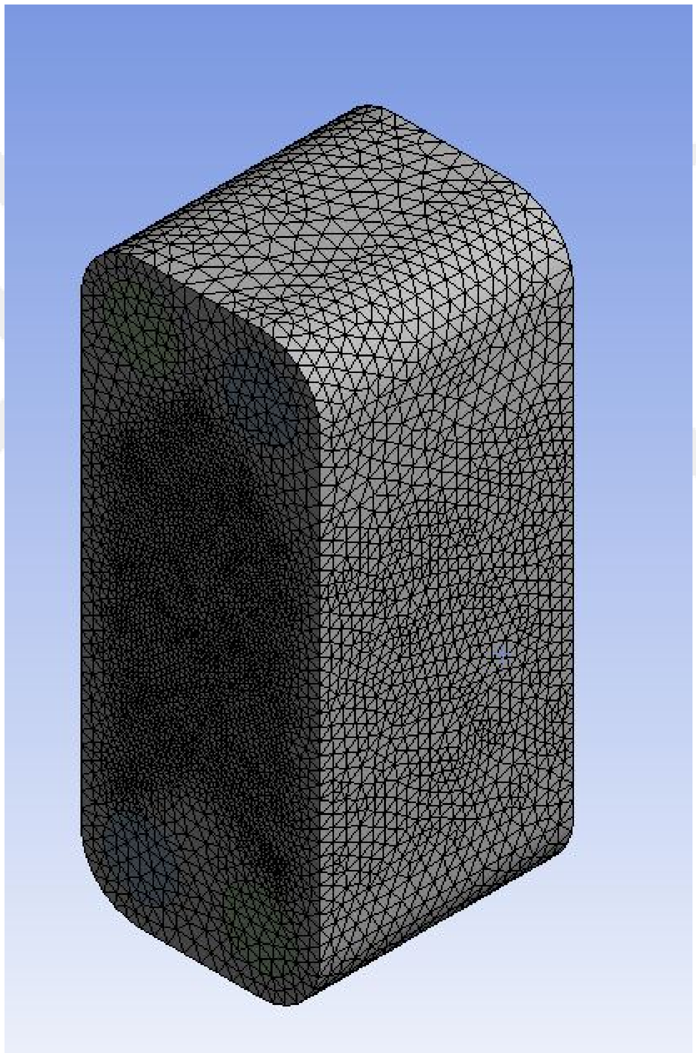

Figure 3.3: Grid generation of the model

The solution independence is applied by checking the grid-dependency for three different grids: 1032514, 1975234, 2435012, 2925143, and 3125214 cells, respectively. It is indicated that the error %age decrease with increasing number of grids where the error percentages of hot water outlet temperature are 1.73%, 1.32%, 0.60%, 0.20%, and 0.09% for 1032514, 1975234, 2435012, 2925143, and 3125214 cells cell numbers so that the number of 3125214 cells were chosen for the simulation.

Table 3: Error %age of hot water temperature

Meshing elements number	Hot water temperature (K)	Error%
1032514	320.0	1.73%
1975234	318.0	1.32%
2435012	315.0	0.60 %
2925143	314.5	0.20%
3125214	314.3	0.09 %

3.4 CFD PROCEDURE AND BOUNDARY CONDITIONS

Commercial software is utilized for setting up and applying the energy and mass calculations at the steady state case. Through the gravity influence and realizable k-Ɛ for the viscid improved wall function porotype, the pressure-based solver was selected. The discrete step was introduced to model the nanoparticles with water, activating continuous phase contact and updating at each iteration. The simulation iterations numbers increase until the mass continuity, speed stream, energy, turbulent viscosity, and separate phase solution residuals reach the minimum values. A simple structure is designated for coupling the pressure and the velocity. The second-order unwinding arrangement is critical for discrete advective terms for example momentum, strength, and turbulent equations of kinetic energy. For boundary conditions, velocity inlet is measured at the inlet of the hot and cold water domains of the PHE with the essential values where the temperature at the inlet of hot and cold water is performed at 333 K and 299 K, respectively. The turbulent range is achieved with *Re* from 2540 to 12700. The outlets of hot and cold water flows are set at pressure outlet condition and the values equal to zero gauge pressure with the no-slip condition. All the external surfaces are set at zero heat flux and the whole model is initialized at 299 K where Table 4 shows the numerical boundary conditions.

Table 4: Initial and boundary conditions

	Values
Inlet hot water temperature	333 K
Inlet cold water temperature	299 K
Pressure outlet of hot water	Atmospheric pressure (101325 Pa)
Pressure outlet of cold water	Atmospheric pressure (101325 Pa)
Heat flux of outer surfaces	0.0
Range of *Re*	2540 to 12700
Hot water mass flow rates	12, 14, 16, 18 LPM
Cold water mass flow rates	12 LPM

3.5 GOVERNING EQUATIONS

The governing equation utilized in this study for showing fluid behaviors inside the PHE has been introduced in this section. The governing equations for continuity, momentum, energy in the CFD are presented as following [34]:

Continuity expression:

$$\frac{\partial}{\partial x_i}(\rho u_i) = 0 \tag{1}$$

Momentum expression:

$$\frac{\partial}{\partial x_i}(\rho u_i u_k) = \frac{\partial p}{\partial x_i} + \frac{\partial}{\partial x_i}(\mu \frac{\partial u_k}{\partial x_i}) \tag{2}$$

Energy expression:

$$\frac{\partial}{\partial x_i}(\rho u_i T) = \frac{\partial}{\partial x_i}(\frac{\partial T}{\partial x_i}\frac{k}{C_P}) \tag{3}$$

Moreover, u is the velocity vector, ρ is the density and μ is the viscosity. Moreover *k* is the thermal conductivity, *T* is the temperature and C_p is the specific heat.

3.6 TURBULENCE MODEL

The fluid flow in the PHE is turbulent due to the water flow, velocity, and heat transfer. The time averaged special influences of the turbulence levels on the parameters are examined using the Favre-averaged Navier-Stokes expressions. Conveyance calculations for turbulent kinetic energy are needed to complete this system of equations. In the examined fluid flow and heat transfer investigation, the selected model fulfills the accuracy and reliability requirements. Turbulent kinetic energy *k* equation:

$$\frac{\partial}{\partial t}(\rho k) + \frac{\partial}{\partial x_i}(\rho k u_i) = \frac{\partial p}{\partial x_j}\left(\alpha_k \mu_{eff} \frac{\partial k}{\partial x_j}\right) - \rho\varepsilon + G_k \tag{4}$$

Turbulent kinetic energy Ɛ equation:

$$\frac{\partial}{\partial t}(\rho\varepsilon) + \frac{\partial}{\partial x_i}(\rho\varepsilon u_i) = \frac{\partial}{\partial x_j}\left(\alpha_\varepsilon \mu_{eff} \frac{\partial k}{\partial x_j}\right) + C_{1\varepsilon}{}^{*}\frac{\varepsilon}{k}G_K - C_{2\varepsilon}\rho\frac{\varepsilon^2}{k} \tag{5}$$

The experimental factors for the RNG k-ε model are assigned [35].

$$C_\mu = 0.0845\,, C_{1\varepsilon}{}^{*} = 1.42, C_{2\varepsilon}{}^{*} = 1.68, \beta = 0.012$$

Where G_k is the eddy viscosity, μ_{eff} is the effective turbulent viscosity and the quantities α_k and α_ϵ are the opposite operative Prandtl numbers for k and ϵ, respectively

3.7 DYNAMIC DATA

In a heat exchanger, the emitted heat from the hot fluid equals the absorbing heat from the cold fluid, and the heat amounts for the hot and cold fluids may be computed using:

$$Q_h = m_h C_{p,h}\left(T_{h,in} - T_{h,out}\right) \tag{6}$$

$$Q_c = m_c C_{p,c}\left(T_{c,out} - T_{c,in}\right) \tag{7}$$

m_h and m_c is the hot and cold flow rates sides, respectively and C_p is the specific heat of water. Q_{ave} symbolizes the hot and the cold fluid the main heat power and is considered by:

$$Q_{ave} = \frac{Q_h + Q_c}{2} \tag{8}$$

And the logarithmic mean temperature (LMTD) can be calculated by [34]:

$$LMTD = \frac{(T_{h,out} - T_{c,in}) - (T_{h,in} - T_{c,out})}{\ln\frac{(T_{h,out} - T_{c,in})}{(T_{h,in} - T_{c,out})}} \tag{9}$$

A symbolizes the whole heat transfer area and T is the temperature so that the *U* can be indicated by [36]:

$$U = \frac{Q_{ave}}{A \cdot LMTD} \tag{10}$$

The *Re* can be defined by the equation:

$$Re = \frac{\rho v D}{\mu} \tag{11}$$

Where V is the velocity, μ is the viscosity and ρ is the density and the *Nu* may be defined by:

$$Nu = \frac{h\, D_h}{k} \tag{12}$$

D_h is the hydraulic diameter and k is the thermal conductivity. The *f* depends on the *ΔP* and geometry of the tube and may be defined by [37].

$$f = \frac{\Delta P}{\rho \frac{l}{D_h} \frac{V^2}{2}} \tag{13}$$

l is the space between the centroid of the suction and discharge is referred to as the port to port distance and ΔP is the pressure drop.

The exergy losses can be determined by:

$$E = E_h + E_c \quad (14)$$

Moreover E_c and E_h are the exergy changes of cold and hot fluids, respectively. both may be defined by those equations [38]:

$$E_h = T_o \left[m_h \left(s_{h,out} - s_{h,in} \right) + \frac{Q_h}{T_{surr}} \right] \quad (15)$$

$$E_c = T_o \left[m_h \left(s_{c,out} - s_{c,in} \right) - \frac{Q_c}{T_{surr}} \right] \quad (16)$$

Where T_o is the ambient temperature and s is the entropy where T_{surr} is the surrounding temperature.

3.8 MODEL VALIDATION

For confirmation of the numerical outcomes, the U of the current work was associated with the earlier investigational work [31]. Figure 3.4 explains the relation between the U of the plate heat versus the Re for the numerical and experimental studies.

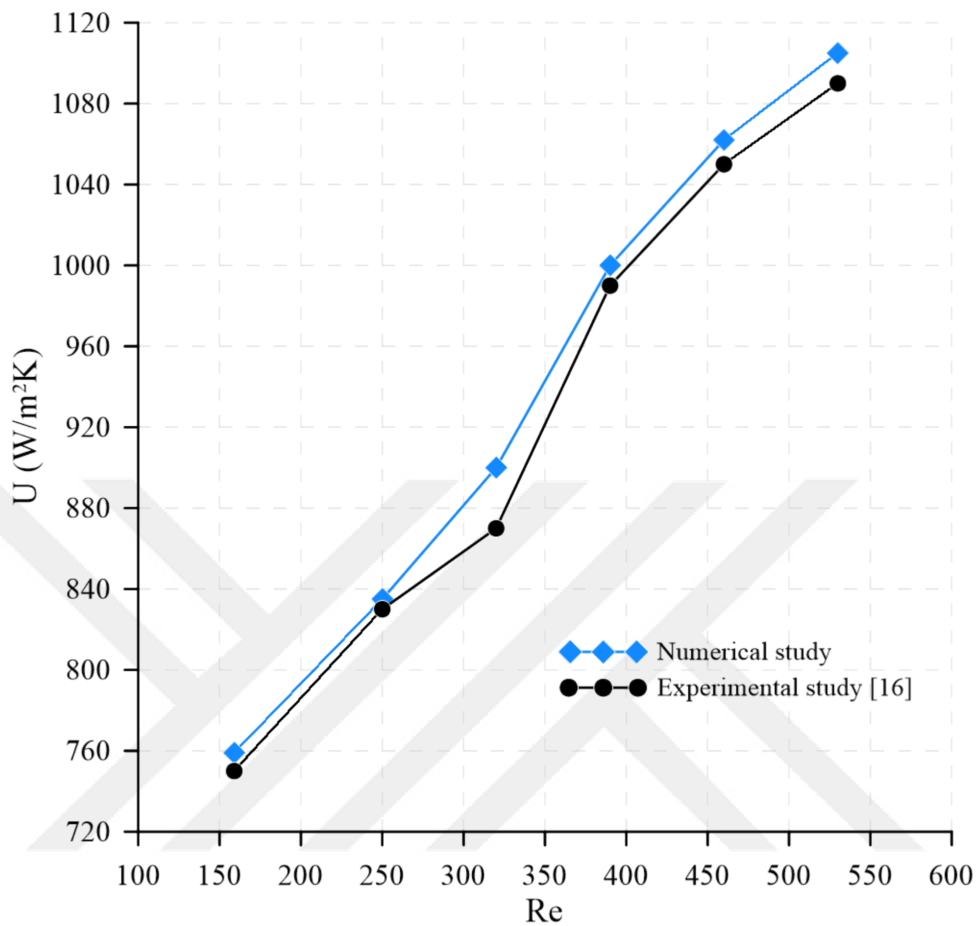

Figure 3.4: Comparison of numerical and experimental studies for validation

The variation between the findings is indicated to be very small. The present numerical results have adequate practical precision. For the *U*, the normal variations between numerical and experimental results are about 3.94%. For the general heat transfer coefficient, the highest dissimilarity is 8.01% and the lowest dissimilarity is 2.64% the findings of the validation explained that the variations are appropriate between the numerical results and the experimental results.

4. RESULTS AND DISCUSSIONS

In this section, the *U*, *Nu*, *f*, and exergy losses are illustrated for the *Re* range from 2540 to 12700. Figure 4.1 displays the relation between the *U* of the Tin nanofluids with dissimilar weight fractions (0.1%, 0.2%, 0.3%, 0.4, 0.5%, and 0.6%) and *Re* with distilled water case.

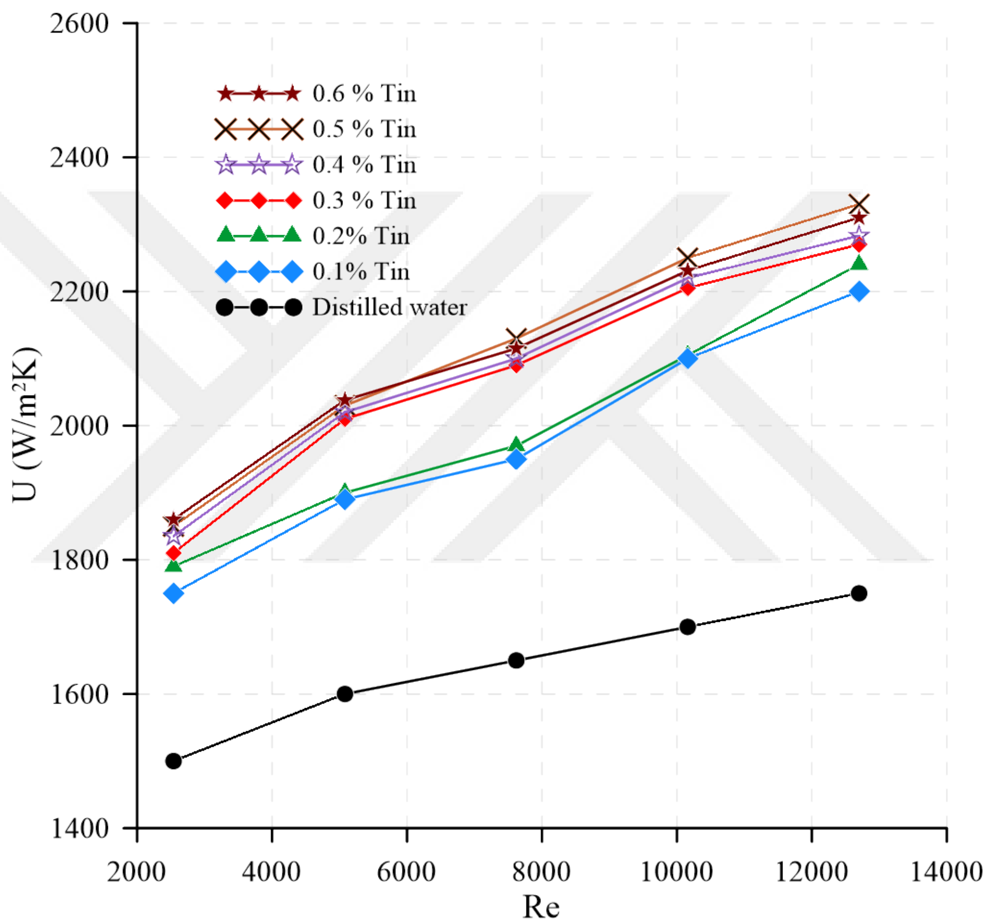

Figure 4.1: The *U* of Tin nanofluids at several mass fraction and pure water versus Re

It is indicated that *U* increased with the rise of *Re*s and weight fraction of nanoparticles where the nanofluids with 0.5% concentration achieved the highest *U*. The figure displays the special influences of nanofluids on heat transfer comparing to distilled water. It can be indicated that in the case of 0.6% concentration, the *U* has a higher value comparing to 0.5% volume concentration with low *Re* then the heat transfer coefficient has lower concentrations with high *Re*. That can be explained as the concentration increases in case of high *Re*s the solid nanoparticles can't have the time to store the heat and transfer it to the water. Figure 4.2 explains the *U* ratio of Tin nanofluids at various weight fractions versus Re.

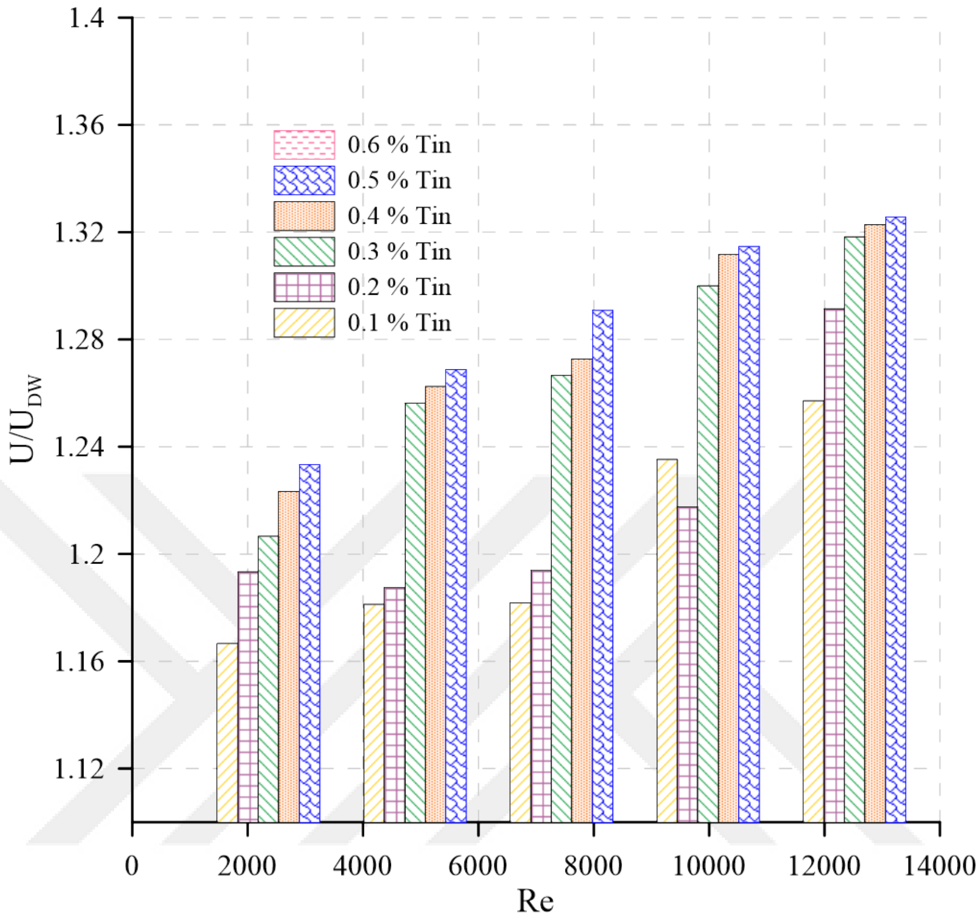

Figure 4.2: The *U* ratio of Tin nanofluids at several weight fraction versus Re

U ratios for 0.1% , 0.2% , 0.3% , 0.4 , 0.5% and 0.6% weight concentration of Tin nanofluids are between (117%-126%) , (118%-130%), (121%-132%) , (123%-133%) , (123.5%-133.5%) and (124%-130%) respectively. The extreme augmentation in heat transfer factor occurred with the 0.5% nanofluids concentrating following the figures of 123.5%-133.5%. This can be explained as the increase in the *Re*s leads to further serious nanoparticle engagements and a higher speed change among the Tin particles with 300 μm and the base water fluid. Besides, the thermal conductivity of the working fluids enhances with the addition of nanoparticles, and the thermal conductivity of the Tin nanofluid grows while the nanoparticle concentration rises. Figure 4.3 displays the relation between the *Nu* of different concentrations of nanoparticles of Tin with a water base and distilled water versus the *Re*s.

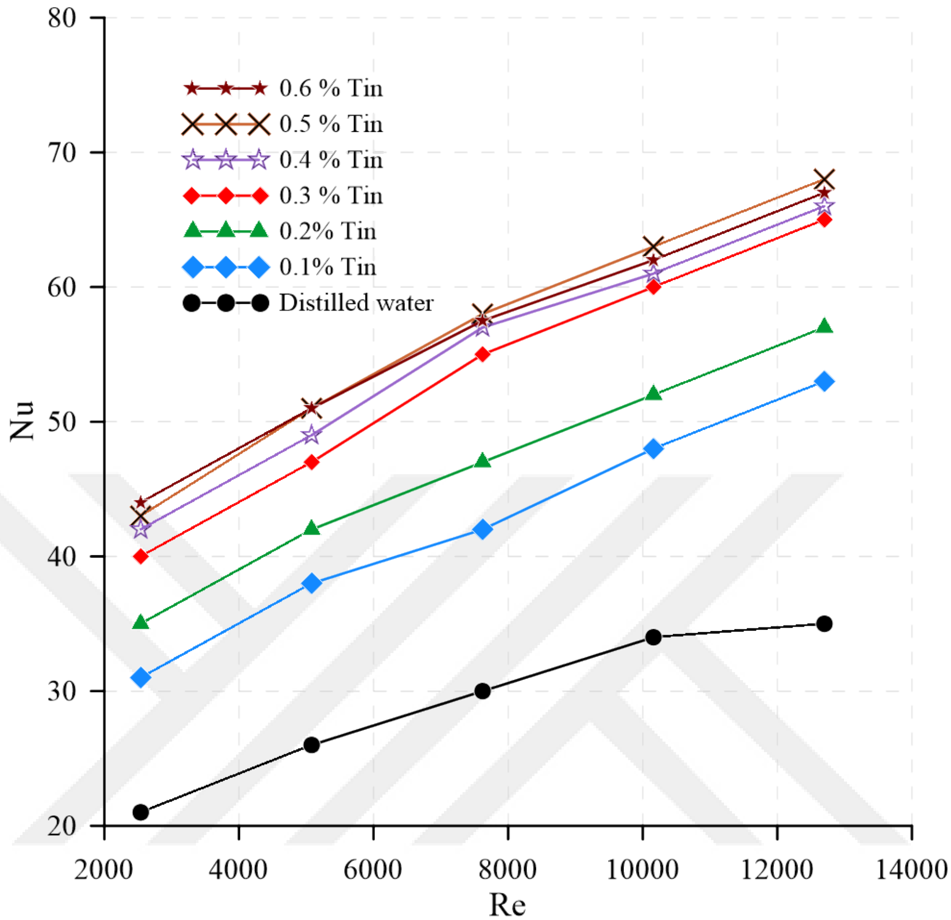

Figure 4.3: *Nu* of Tin nanofluids at various mass fraction and pure water versus Re

It is observed that the *Nu* enhances with the growth of the Reynold figure and capacity concentration of nanofluids. The 0.5 wt.% Tin-water nanofluid scores the maximum values of *Nu* from 43 to 68. It may be explained that the nanoparticles rise the *Nu* comparing with pure water as the heat transfer grows with the rise of the nanofluid concentration in water until the concentration reaches 0.5 wt.%.

The *f* of Tin nanofluids at several mass fractions 0.1%, 0.2%, 0.3%, 0.4, 0.5% and 0.6 and distilled water is displayed in Figure 4.4. The *f* of each case with and without nanofluids drops with the increase of *Re*. The case of 0.6% concentration Tin to water scored the maximum *f* with values from 0.18 to 0.35 becautilizing of the increase of resistance of the fluid to motion as the viscosity increase with the nanoparticles concentration increase.

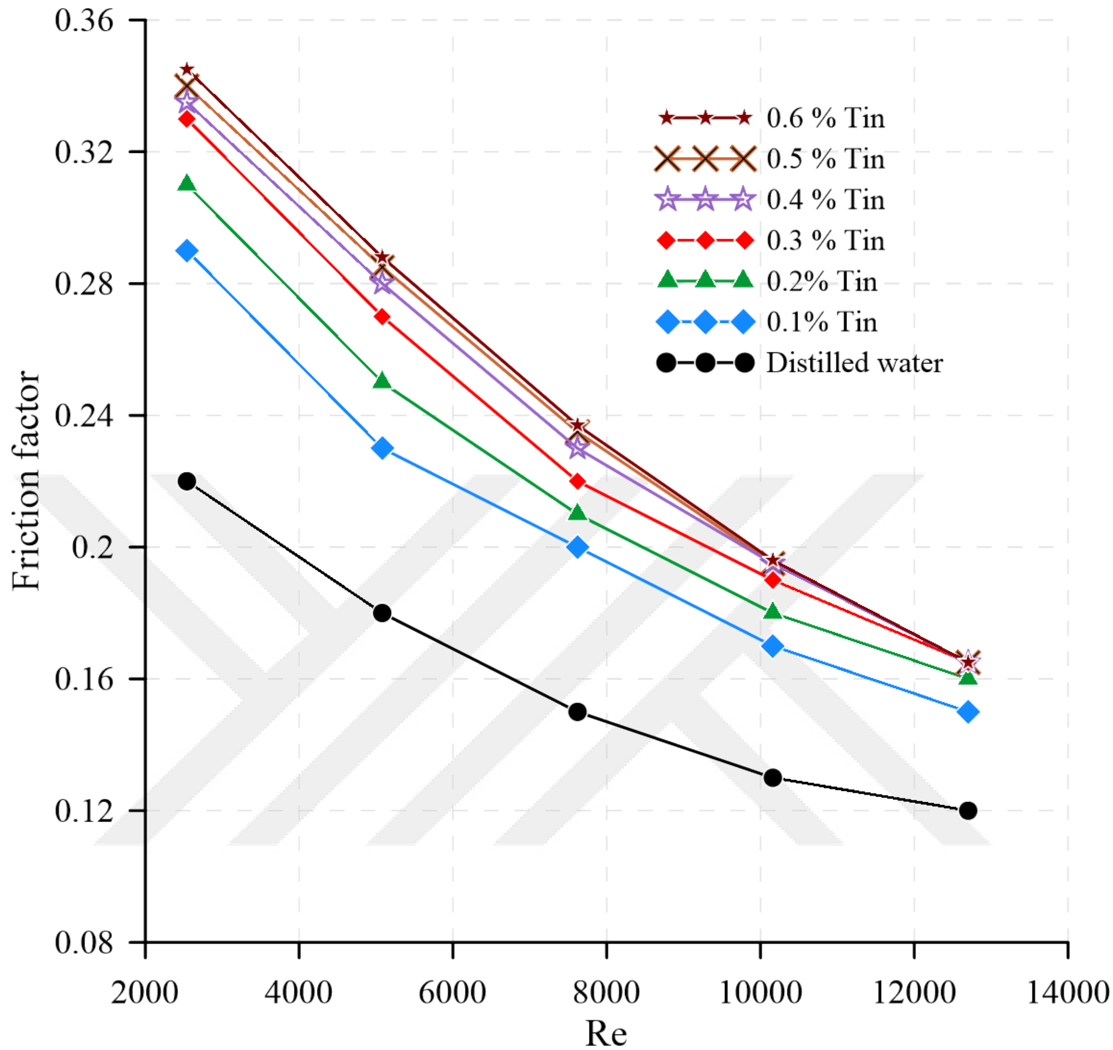

Figure 4.4: The *f* of Tin nanofluids at several mass fraction and pure water versus Re

The exergy losses of Tin nanofluids at several mass fractions 0.1%, 0.2%, 0.3%, 0.4, 0.5% and 0.6 and distilled water are investigated in Figure 4.5.

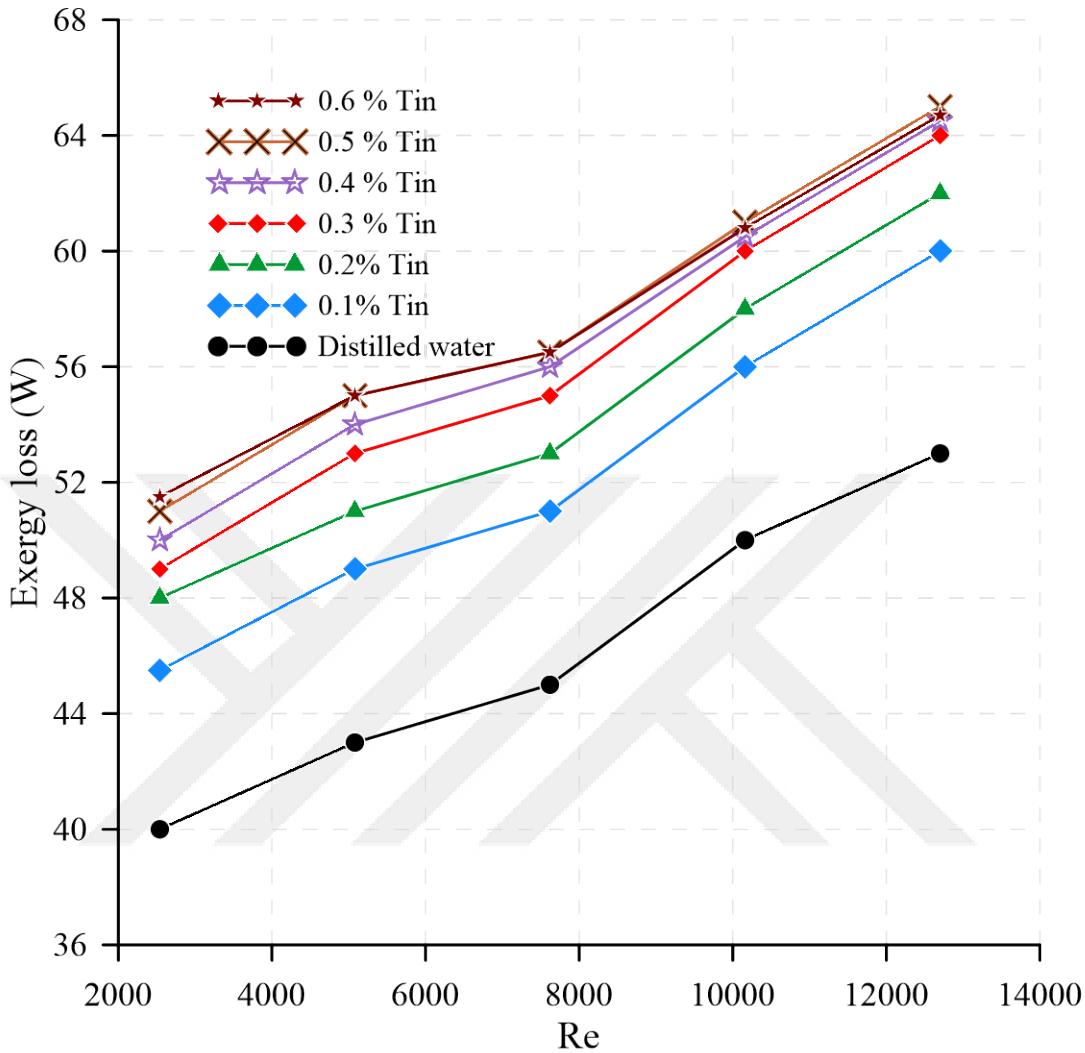

Figure 4.5: The exergy loss of Tin nanofluids at many mass fraction and pure water versus Re

It may be observed that the exergy loss of nanofluid with different concentrations rise with the increase of *Re*. Nanoparticles of Tin with water increase the exergy losses comparing to distilled water. The concentration of 0.5 wt. % Tin –water achieved the highest rate of exergy loss following the numbers from 50 to 66. Figure 4.6 shows the streamlines of cold water with temperature distribution where the temperature of the old water increases inside the tubes where the highest temperature appears at the outlet of the cold water pass. The flow inside the PHE is counter so that the quantity of heat that transferred from the hot side to the cold water enhanced comparing with parallel flow.

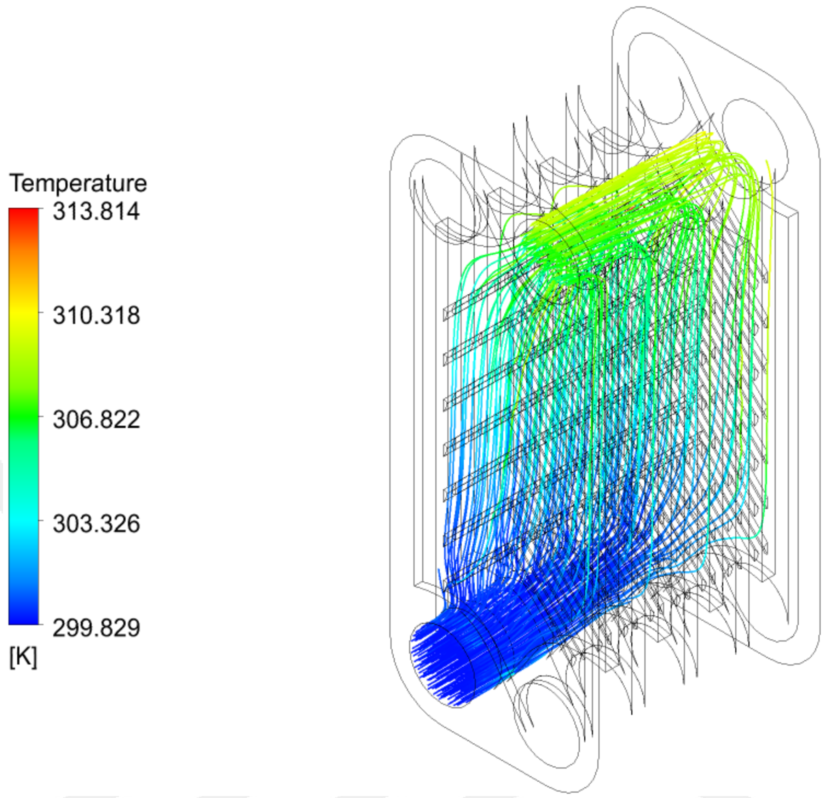

Figure 4.6: Temperature distribution for the cold water side

Figure 4.7 explains the temperature distribution of nanofluid of Tin and water inside the hot side where the temperature decreases inside the passes between the plates. It can be explained that the streamlines show the smooth motion of hot water with nanoparticles from the upper tube to the down tube. It is indicated that the temperature distribution is uniform besides the plates as the corrugations angle force the flow to have a regular paths so that the heat transfer factors are extensively improved.

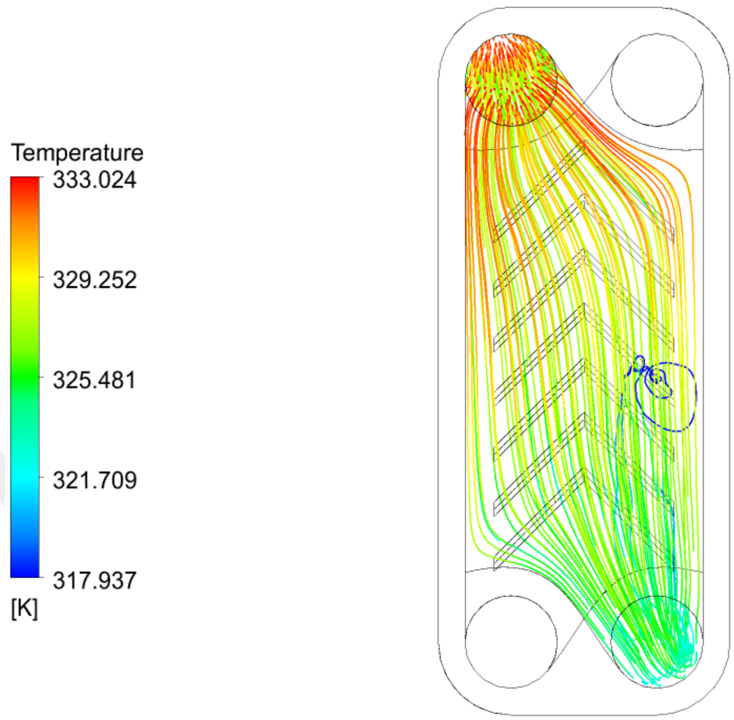

Figure 4.7: Temperature distribution for the hot water side

The velocity distribution of the cold from many views is explained in Figure 4.8 and Figure 4.9 where great turbulence level has been perceived in the gab produced by the extreme vortex shaped by the streams. It can explained that the velocity increased inside the plates so that the turbulence levels enhanced as well as the nanoparticles improves the thermal and the hydraulic performances in the PHE. It can indicated that the velocity decreased inside the upper pipe so that the mixture reaches the last gab of plates with lesser velocity comparing to the first one so the velocity in the last stages of PHE is less than the earlier stages.

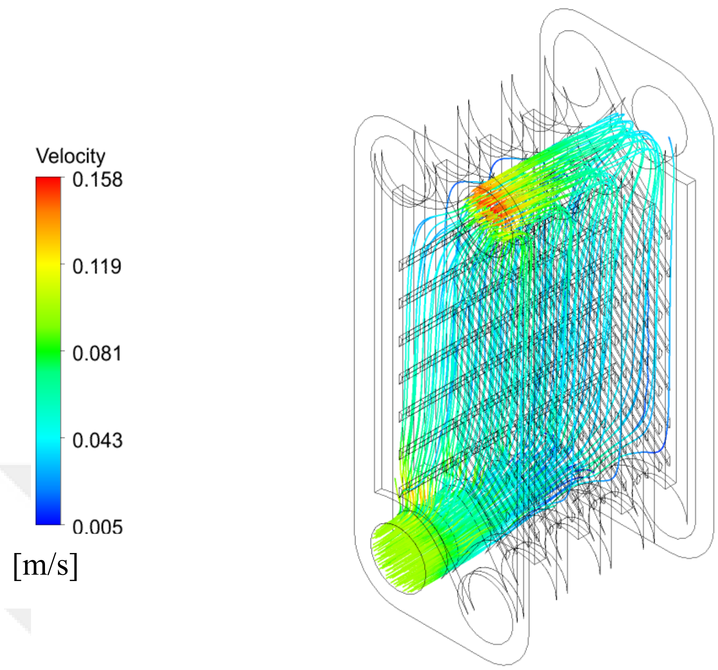

Figure 4.8: Velocity distribution of cold water

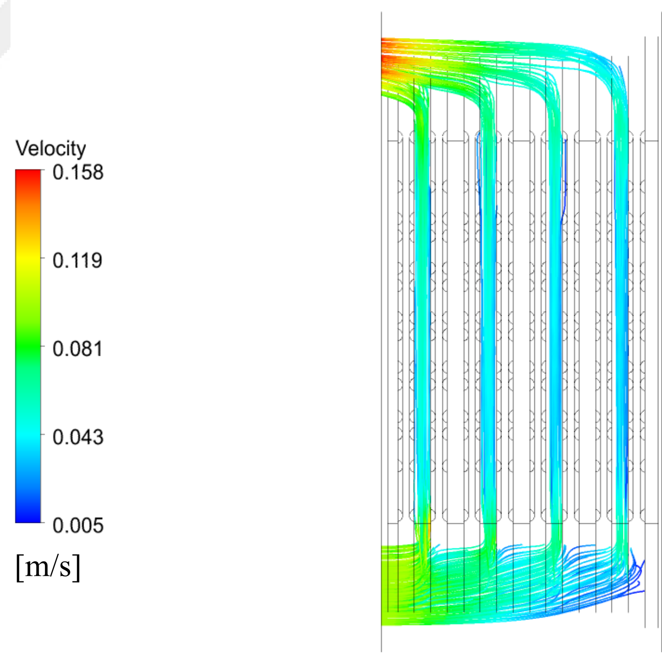

Figure 4.9: Velocity distribution of cold water

Velocity streamlines of Tin with water nanofluids are explained in Figure 4.10 where the hot water with solid particles moves between the plates uniformly. Thanks to corrugations on the plate, which induce a rapid shift in flow directions, significant turbulence has also been recorded at the confluence of the distribution space and the heat transfer region. Becautilizing it encounters more impediment in the heat transfer region than in the distribution area, fluid velocity drops as it travels through it.

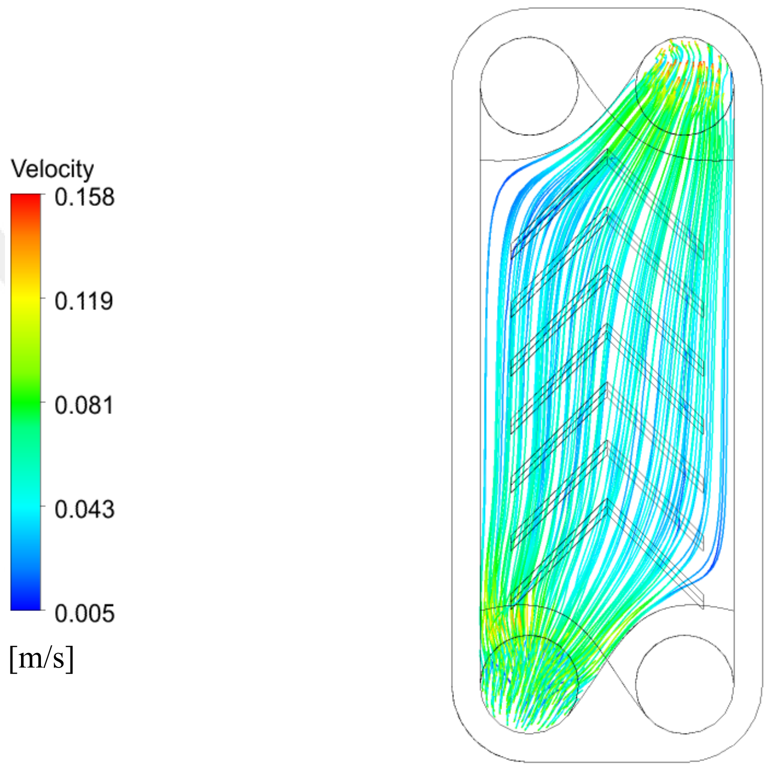

Figure 4.10: Velocity distribution of hot water with nanofluids

Figure 4.11 shows the gage pressure distribution of the hot side that consists of nanoparticles and hot water. The pressure has the maximum values at the inlet of hot side after that the pressure decrease inside the plate gabs. It is indicated that the ΔP in the back plates is upper than the ΔP for the front plates. The ΔP rises with the mass flow rate and thus the pumps power rises since the growth in stream rate involves a higher ΔP. The reasons of increase the ΔP inside the PHE are the friction between the water and the plates , frictions between the nanobarticles and the plates , and friction resulted from the flow over the corrugated angles inside the heat exchanger.

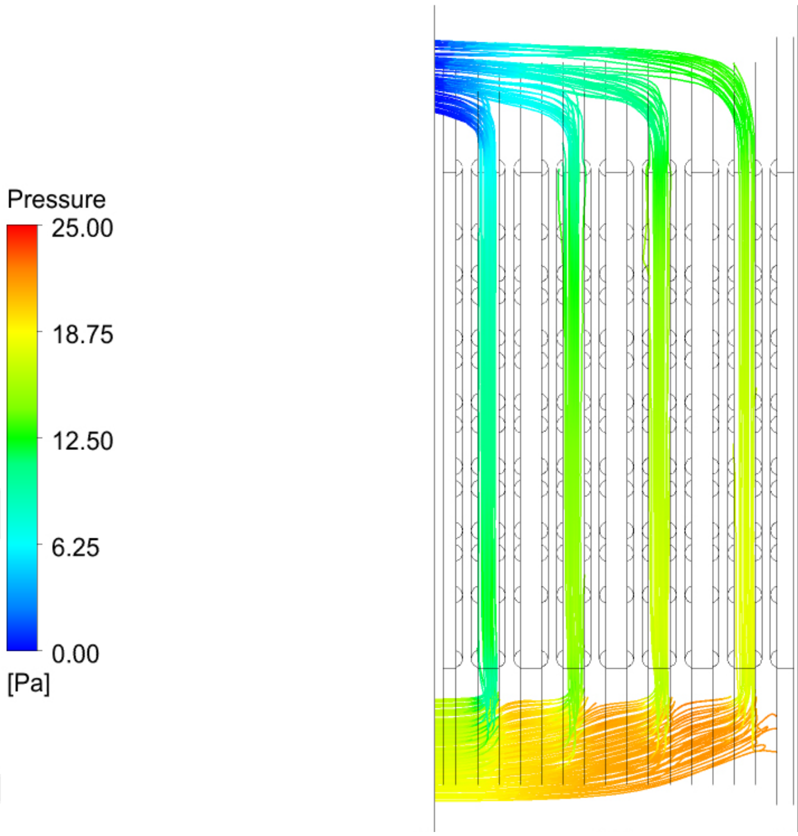

Figure 4.11: Pressure distribution cross the PHE

5. CONCLUSIONS

In the current investigation, heat transfer, *ΔP*, and exergy losses features of Tin nanofluid in a counter flow PHE were studied using a numerical modelling and confirmed with investigational results. The research was completed for a range of solid particles weight concentrations (0.1, 0.2, 0.3, 0.4, 0.5, and 0.6 wt. %), *Re* from 2540 to 12700 to achieve the turbulent level. Established by the outcomes and discussion, the next conclusions may be prepared:

a. *U* increased with the rise of *Re*s and weight fraction of nanoparticles where the nanofluids with 0.5% concentration achieved the highest values and the enhancement ratio %age start from 123.5%-133.5%.
b. *Nu* enhance with the growth of the Reynold number and volume concentration of nanofluids where the 0.5 wt.% Tin-water nanofluid scores the highest values of *Nu* from 43 to 68.
c. The *f* decreases with the increase of *Re* where the case of 0.6% concentration Tin to water recorded the extreme *f* with values from 0.18 to 0.35.

d. The exergy loss of nanofluid with different concentrations rises with the growth of *Re* and the concentration of 0.5 wt. % Tin –water achieved the highest exergy loss following the numbers from 50 to 66.

e. Streamlines and contours of temperature, velocity, and pressure distribution inside the PHE give reliable explanations for the motion of cold and hot water and heat transfer enhancement.

6. FUTURE STUDY

The study of the thermal and hydraulic performance of PHE with novel nano solid particles and air injection may be advised for the future studies.

REFERENCES

[1] T. K. Hou, S. N. Kazi, A. B. Mahat, C. B. Teng, A. Al-Shamma'a, and A. Shaw, "Industrial Heat Exchanger: Operation and Maintenance to Minimize Fouling and Corrosion," in Heat Exchangers - Advanced Features and Applications, ed, 2017.

[2] M. Ghalandari, M. I. Shahrestani, A. Maleki, M. S. Shadloo, M. E. H. J. J. o. T. A. Assad, and Calorimetry, "Applications of intelligent methods in various types of heat exchangers: a review," pp. 1-12, 2021.

[3] F. A. Mota, E. Carvalho, M. J. H. T. S. Ravagnani, and Applications, "Modeling and design of PHE," 2015.

[4] H. Ibrahim, N. Sazali, A. S. M. Shah, M. S. A. Karim, F. Aziz, W. N. W. J. J. o. A. R. i. F. M. Salleh, et al., "A review on factors affecting heat transfer efficiency of nanofluids for application in PHE," vol. 60, pp. 144-154, 2019.

[5] N. Stoitchkov and G. J. I. j. o. r. Dimitrov, "Effectiveness of crossflow PHE for indirect evaporative cooling: Efficacité des échangeurs thermiques à plaques, à courants croises pour refroidissement indirect évaporatif," vol. 21, pp. 463-471, 1998.

[6] S. K. Das and W. J. C. Roetzel, "Second law analysis of a PHE with an axial dispersive wave," vol. 38, pp. 791-798, 1998.

[7] A. Muley and R. Manglik, "Experimental study of turbulent flow heat transfer and ΔP in a PHE with chevron plates," 1999.

[8] W. Y. Saman and S. J. S. E. Alizadeh, "Modelling and performance analysis of a cross-flow type PHE for dehumidification/cooling," vol. 70, pp. 361-372, 2001.

[9] B. Prabhakara Rao, P. Krishna Kumar, and S. K. Das, "Effect of flow distribution to the channels on the thermal performance of a PHE," Chemical Engineering and Processing:

Process Intensification, vol. 41, pp. 49-58, 2002/01/01/ 2002. Available: https://www.sciencedirect.com/science/article/pii/S0255270101001052

[10] Z. H. J. H. t. e. Ayub, "PHE literature survey and new heat transfer and *ΔP* correlations for refrigerant evaporators," vol. 24, pp. 3-16, 2003.

[11] D. Wen, Y. J. J. o. t. Ding, and h. transfer, "Effective thermal conductivity of aqueous suspensions of carbon nanotubes (carbon nanotube nanofluids)," vol. 18, pp. 481-485, 2004.

[12] J. Koo and C. Kleinstreuer, "Laminar nanofluid flow in microheat-sinks," International Journal of Heat and Mass Transfer, vol. 48, pp. 2652-2661, 2005/06/01/ 2005. Available: https://www.sciencedirect.com/science/article/pii/S0017931005001328

[13] F. C. C. Galeazzo, R. Y. Miura, J. A. W. Gut, and C. C. Tadini, "Experimental and numerical heat transfer in a PHE," Chemical Engineering Science, vol. 61, pp. 7133-7138, 2006/11/06/ 2006. Available: http://www.sciencedirect.com/science/article/pii/S0009250906004532

[14] G. A. Longo and A. Gasparella, "Heat transfer and *ΔP* during HFC refrigerant vaporisation inside a brazed PHE," International Journal of Heat and Mass Transfer, vol. 50, pp. 5194-5203, 2007/12/01/ 2007. Available: https://www.sciencedirect.com/science/article/pii/S0017931007004371

[15] F. S. K. Warnakulasuriya and W. M. Worek, "Heat transfer and *ΔP* properties of high viscous solutions in PHEs," International Journal of Heat and Mass Transfer, vol. 51, pp. 52-67, 2008/01/01/ 2008. Available: https://www.sciencedirect.com/science/article/pii/S0017931007003730

[16] A. G. Kanaris, A. A. Mouza, and S. V. Paras, "Optimal design of a PHE with undulated surfaces," International Journal of Thermal Sciences, vol. 48, pp. 1184-1195, 2009/06/01/ 2009. Available: http://www.sciencedirect.com/science/article/pii/S1290072908002251

[17] C.-S. Jwo, L.-Y. Jeng, T.-P. Teng, C.-C. J. J. o. A. Chen, and Compounds, "Performance of overall heat transfer in multi-channel heat exchanger by alumina nanofluid," vol. 504, pp. S385-S388, 2010.

[18] M. A. Ahmed, N. H. Shuaib, M. Z. Yusoff, and A. H. Al-Falahi, "Numerical investigations of flow and heat transfer enhancement in a corrugated channel using nanofluid," International Communications in Heat and Mass Transfer, vol. 38, pp. 1368-1375, 2011.

[19] M. Taws, C. T. Nguyen, N. Galanis, and I. Gherasim, "Experimental investigation of nanofluid heat transfer in a PHE," in Heat Transfer Summer Conference, 2012, pp. 1-8.

[20] A. K. Tiwari, P. Ghosh, and J. Sarkar, "Performance comparison of the PHE using different nanofluids," Experimental Thermal and Fluid Science, vol. 49, pp. 141-151, 2013/09/01/ 2013. Available: https://www.sciencedirect.com/science/article/pii/S0894177713001015

[21] A. K. Tiwari, P. Ghosh, J. Sarkar, H. Dahiya, and J. Parekh, "Numerical investigation of heat transfer and fluid flow in PHE using nanofluids," International Journal of Thermal Sciences, vol. 85, pp. 93-103, 2014.

[22] V. Kumar, A. K. Tiwari, and S. K. Ghosh, "Application of nanofluids in PHE: A review," Energy Conversion and Management, vol. 105, pp. 1017-1036, 2015/11/15/ 2015. Available: http://www.sciencedirect.com/science/article/pii/S0196890415008079

[23] D. Huang, Z. Wu, and B. Sunden, "Effects of hybrid nanofluid mixture in PHEs," Experimental Thermal and Fluid Science, vol. 72, pp. 190-196, 2016/04/01/ 2016. Available: https://www.sciencedirect.com/science/article/pii/S0894177715003325

[24] V. Kumar, A. K. Tiwari, and S. K. Ghosh, "Characterization and performance of nanofluids in PHE," Materials Today: Proceedings, vol. 4, pp. 4070-4078, 2017/01/01/ 2017. Available: https://www.sciencedirect.com/science/article/pii/S2214785317305205

[25] S. H. Pourhoseini, N. Naghizadeh, and H. Hoseinzadeh, "Effect of silver-water nanofluid on heat transfer performance of a PHE: An experimental and theoretical study," Powder Technology, vol. 332, pp. 279-286, 2018/06/01/ 2018. Available: https://www.sciencedirect.com/science/article/pii/S0032591018302511

[26] M. Shirzad, S. S. M. Ajarostaghi, M. A. Delavar, and K. Sedighi, "Improve the thermal performance of the pillow PHE by using nanofluid: Numerical simulation," Advanced Powder Technology, vol. 30, pp. 1356-1365, 2019.

[27] A. Abbas, H. Lee, A. Sengupta, and C.-C. Wang, "Numerical investigation of thermal and hydraulic performance of shell and PHE," Applied Thermal Engineering, vol. 167, 2020.

[28] N. S. Pandya, H. Shah, M. Molana, and A. K. Tiwari, "Heat transfer enhancement with nanofluids in PHEs: A comprehensive review," European Journal of Mechanics - B/Fluids, vol. 81, pp. 173-190, 2020.

[29] S. Al zahrani, M. S. Islam, and S. C. Saha, "Heat transfer enhancement investigation in a novel flat PHE," International Journal of Thermal Sciences, vol. 161, p. 106763, 2021/03/01/ 2021. Available:

https://www.sciencedirect.com/science/article/pii/S1290072920312072

[30] S. Singh, P. Verma, S. K. J. I. J. o. N. M. f. H. Ghosh, and F. Flow, "Numerical and experimental analysis of performance in a compact PHE using graphene oxide/water nanofluid," 2021.

[31] R. Barzegarian, M. K. Moraveji, and A. Aloueyan, "Experimental investigation on heat transfer characteristics and *ΔP* of BPHE (brazed PHE) using TiO 2 –water nanofluid," Experimental Thermal and Fluid Science, vol. 74, pp. 11-18, 2016/06/01/ 2016. Available: https://www.sciencedirect.com/science/article/pii/S0894177715003416

[32] Y. Yin, L. Hang, S. Zhang, and X. L. Bui, "Thermal oxidation properties of titanium nitride and titanium–aluminum nitride materials — A perspective for high temperature air-stable solar selective absorber applications," Thin Solid Films, vol. 515, pp. 2829-2832, 2007/01/22/ 2007. Available: https://www.sciencedirect.com/science/article/pii/S0040609006004822

[33] R. R. Ansys® Academic Research Mechanical, Help System, Coupled Field Analysis Guide, ANSYS, Inc.

[34] A. A. Abbasian Arani and R. Moradi, "Shell and tube heat exchanger optimization using new baffle and tube configuration," Applied Thermal Engineering, vol. 157, 2019.

[35] Y. Lei, Y. Li, S. Jing, C. Song, Y. Lyu, and F. Wang, "Design and performance analysis of the novel shell-and-tube heat exchangers with louver baffles," Applied Thermal Engineering, vol. 125, pp. 870-879, 2017.

[36] S. A. Marzouk, M. M. Abou Al-Sood, M. K. El-Fakharany, and E. M. S. El-Said, "Thermo-hydraulic study in a shell and tube heat exchanger using rod inserts consisting of wire-nails with air injection: Experimental study," International Journal of Thermal Sciences, vol. 161, p. 106742, 2021/03/01/ 2021. Available:

https://www.sciencedirect.com/science/article/pii/S1290072920311868

[37] B. Saleh and L. S. Sundar, "Experimental study on heat transfer, *f*, entropy and exergy efficiency analyses of a corrugated PHE using Ni/water nanofluids," International Journal of Thermal Sciences, vol. 165, p. 106935, 2021/07/01/ 2021. Available: https://www.sciencedirect.com/science/article/pii/S1290072921001010

[38] S. A. Marzouk, M. M. Abou Al-Sood, E. M. S. El-Said, and M. K. El-Fakharany, "Effect of wired nails circular–rod inserts on tube side performance of shell and tube heat exchanger: Experimental study," Applied Thermal Engineering, vol. 167, p. 114696, 2020/02/25/ 2020. Available: https://www.sciencedirect.com/science/article/pii/S1359431119348501